



## Full Length Article

# Study of heavy metals adsorption using a silicate-based material: Experiments and theoretical insights

Lisdelys González-Rodríguez<sup>a,b</sup>, Yoan Hidalgo-Rosa<sup>c,d</sup>, Julio Omar Prieto García<sup>e</sup>, Manuel A. Treto-Suárez<sup>f</sup>, Karel Mena-Ulecia<sup>g,h</sup>, Osvaldo Yañez<sup>b,\*</sup>

<sup>a</sup> Facultad de Ingeniería y Negocios, Universidad de Las Américas, Concepción, 4030000, Chile

<sup>b</sup> Núcleo de Investigación en Data Science (NIDS), Facultad de Ingeniería y Negocios, Universidad de Las Américas, Santiago 7500975, Chile

<sup>c</sup> Centro de Nanotecnología Aplicada, Facultad de Ciencias, Ingeniería y Tecnología, Universidad Mayor, Camino La Pirámide 5750, Huechuraba, Santiago, Chile, 8580745

<sup>d</sup> Escuela de Ingeniería del Medio Ambiente y Sustentabilidad, Facultad de Ciencias, Ingeniería y Tecnología, Universidad Mayor, Camino La Pirámide 5750, Huechuraba, 8580745 Santiago, Chile

<sup>e</sup> Universidad Central Marta Abreu de las Villas, Departamento de Química y Farmacia, Carretera de Camajuani km 5, Villa Clara, 50100, Cuba

<sup>f</sup> Departamento de Física y Química, Facultad de Ingeniería, IDETECO, Universidad Autónoma de Chile, Av. Alemania 01090, 4810101 Temuco, Chile

<sup>g</sup> Universidad Católica de Temuco, Departamento de Ciencias Biológicas y Químicas, Facultad de Recursos Naturales, Ave. Rudecindo Ortega 02950, Temuco, 4780000, Chile

<sup>h</sup> Núcleo de Investigación en Bioproductos y Materiales Avanzados (BIOMA), Universidad Católica de Temuco, Ave. Rudecindo Ortega 02950, Temuco, 4780000, Chile



## ARTICLE INFO

## Keywords:

Magnesium silicate  
Kinetic study  
Adsorption  
Heavy metals  
Theoretical study

## ABSTRACT

Heavy metal toxicity in water is a serious problem with harmful effects on human health and the ecosystem. This research studied a silicate-based material as an adsorbent for removing four heavy metals from aqueous solutions. The target metal pollutants selected include manganese ( $Mn^{2+}$ ), copper ( $Cu^{2+}$ ), cobalt ( $Co^{2+}$ ), and zinc ( $Zn^{2+}$ ). First, theoretical tools including potential energy surface analysis, Natural Population Analysis, AIM, Wiberg Bond Index, QTAIM, and topological methods offer profound insights into the nature of interactions present in the  $Mg_2O_8Si_3M$  ( $M = Mn^{2+}, Cu^{2+}, Co^{2+}, Zn^{2+}$ ) clusters. Second, the synthesis and characterization of eco-friendly hydrated amorphous magnesium silicate ( $MgOSiO_2nH_2O$ ) was developed. Last, a simple kinetic adsorption test was applied to assess the material selectivity towards heavy metals and support theoretical results. The kinetic adsorption study was analyzed through the pseudo-first and second-order kinetics, Elovich, and the intraparticle diffusion models. The theoretical analysis of the adsorption energies indicates that the adsorption of four metal ions on the  $Mg_2O_8Si_3$  surface is energetically favorable in all cases. The material displayed the following adsorption sequence:  $Cu^{2+}$  ( $59 \text{ mg g}^{-1}$ ) >  $Zn^{2+}$  ( $25 \text{ mg g}^{-1}$ )  $\approx$   $Co^{2+}$  ( $23 \text{ mg g}^{-1}$ ) >  $Mn^{2+}$  ( $15 \text{ mg g}^{-1}$ ). This knowledge can then be used to design and optimize low-cost silicate-based materials for effective heavy metal removal, contributing to efforts to address environmental pollution and protect public health.

## 1. Introduction

The provision of high-quality water should be considered a critical element in maintaining public health [1]. Urban wastewater treatment facilities use various technologies to control pollutants and reduce contaminants in natural aquatic systems [2]. However, as society expands and production escalates, the quantity and diversity of pollution sources have risen, causing the degradation of potable water sources [3]. Industrial wastewater has become a major concern due to the presence of toxic heavy metals [4–6]. These pollutants are not easily

biodegradable and tend to accumulate in living organisms, causing various diseases and disorders. The concentration of heavy metals in industrial wastewater can vary greatly depending on the type of industry. However, here are some typical concentration ranges reported in aquatic ecosystems: lead (Pb): 0.1 - 200 mg/L, cadmium (Cd): 0.1 - 50 mg/L, copper (Cu): 0.2 - 200 mg/L, Zinc (Zn): 1 - 400 mg/L, nickel (Ni): 0.1 - 100 mg/L, chromium (Cr): 0.5 - 250 mg/L, mercury (Hg): 0.01 - 10 mg/L, arsenic (As): 0.1 - 50 mg/L [7,8].

In this framework, metal ions (such as nickel (Ni), barium (Ba), cadmium (Cd), zinc (Zn), nickel (Ni), and copper (Cu), among others)

E-mail addresses: [lgonzalezr@udla.cl](mailto:lgonzalezr@udla.cl) (L. González-Rodríguez), [oyanez@udla.cl](mailto:oyanez@udla.cl) (O. Yañez).

\* Corresponding author.

are toxic species, even at trace levels [4–6]. The toxicity of these metal ions depends on the formed chemical species [9], the concentration levels, and the routes of administration. At determined concentrations, these metal ions are essential for the right functioning of organisms. However, when these concentrations are exceeded, they can be very harmful. For example, when  $\text{Cu}^{2+}$  concentrations are  $<100$  mg, in an adult person, or become excessive, they can produce several diseases (such as Hematological, leukopenia, and neural disorders such as Wilson's, Parkinson's, Menke's, and Alzheimer's are some of the diseases found in human health [8,9]. In the  $\text{Ni}^{2+}$  and  $\text{Co}^{2+}$  cases, unlike  $\text{Cu}^{2+}$ , are required in minimal concentration for the metabolic processes resulting in severe disorders in the respiratory system, central nervous system, the dermis, or even cancer at excessive concentrations [10,11]  $\text{Mn}^{2+}$  can lead to a permanent neurological disorder known as Manganism with symptoms that include tremors, difficulty walking, and facial muscle spasms [12].

In this context, several procedures have been reported to reduce the presence of toxic metals in wastewater [13]. Most techniques used in wastewater are chemical precipitation and filtration, coagulation, oxidation–reduction, electrochemical treatments, reverse osmosis, solvent extraction, and sorption into biological or inorganic materials. The adsorption procedure is an attractive alternative very used for the removal of organic and inorganic impurities. In this sense, the chemistry field research has focused on novel solid materials developed to remove pigments, and metal ions, among others, in wastewater treatment [14–16]. The feasibility of converting different resources such as low-cost materials and revalorizing residues into adsorbents represents an option of economic relevance [6,17,18]. In this sense, novel natural and synthetic sorbents have been investigated [18,19]. In this framework, synthetic silicate-based materials are particularly effective at removing metal ions from water due to their high adsorption capacities and ion exchange properties [20]. Generally, sorbents of silicic origin with good adsorption capacities are effective and less expensive when it comes to treating large volumes of wastewater. This property has led to an increased interest in these silicate-based materials for wastewater treatment [18,21]. For example, sorbents based on natural bentonites [19] reveal that the interaction between  $\text{Ni}^{2+}$  and sorbent has a high rate in the first minutes of contact (20–30 min) and then stabilizes at a constant level. This kinetic parameter is important to reduce the sorption cycle time. The study [22] demonstrated that the affinity of three metals for both types of zeolites followed the order  $\text{Cu}^{2+} > \text{Zn}^{2+} > \text{Mn}^{2+}$ . This means that  $\text{Cu}^{2+}$  had the strongest affinity for the zeolite, followed by  $\text{Zn}^{2+}$ , and then  $\text{Mn}^{2+}$ , an important factor to consider in applications where these metals need to be selectively removed from the solution. Recently, elsewhere reported good properties for  $\text{Al}_2\text{O}_3 \times 3\text{SiO}_2 \times \text{nH}_2\text{O}$  silicate-based material [18]. This material decreased the concentration of several metal ions  $\text{Cr}^{3+}$ ,  $\text{Pb}^{2+}$ ,  $\text{Co}^{2+}$ ,  $\text{Zn}^{2+}$ ,  $\text{Ni}^{2+}$ ,  $\text{Cd}^{2+}$ ,  $\text{Hg}^{2+}$ ,  $\text{Cr}^{4+}$  and  $\text{Cu}^{2+}$  should preferably be physical with the formation of one layer via intraparticle diffusion [18], and until discharge levels permissible in wastewater. In these studies, several kinetic models (such as pseudo-first-order, pseudo-second-order, Elovich, and intraparticle diffusion) were used to understand and optimize the sorption processes. These studies show the good properties of silicate-based materials to remove metal ions. However, the metal/adsorbent interaction was not theoretically supported. In this sense, the theoretical study of the interaction between materials and heavy metal ions [21] is crucial to designing new silicate-based materials with better properties [23,24].

The specific interactions between the metal atoms and the silicate-based material can be attributed to various factors, such as the molecular structures and physicochemical properties of the heavy metals (such as charge or ionic radii), as well as the surface properties of the material. These factors include porous structure (crystallite size), surface area, surface charge/pH, Mg/Si ratio, surface modifications and temperature. [25–28]. Understanding these factors and their effects on the interactions between metal atoms and silicate-based materials is crucial for the design and optimization of materials for heavy metal

removal. This can be achieved through a combination of experimental studies and theoretical modeling.

Theoretical chemistry tools allow the computational study of the metal/silicate-based material interaction and provide a detailed understanding of the adsorption process at the atomic level [29]. In this context, quantum mechanical modeling methods, such as the Quantum Theory of Atoms in Molecules (QTAIM) [30], Wiberg Bond Index (WBI) [31], Independent Gradient Model based on the Hirshfeld partition (IGMH) [32], and Natural population analysis (NPA) [33] are robust tools for accurately studying the interaction between different molecules and a material's surface, which is especially useful in understanding adsorption processes. This method provides a clear and intuitive picture of the interactions in the system, which can be useful for understanding the structure and properties of complex chemical systems [34]. In the research of González-Rodríguez et al. theoretical procedure was developed for examining the interactions and adsorption between activated carbon and several water pollutants [35]. The protocol uses IGMH and AIM (Atoms in molecules) analysis to predict the stability and binding mechanisms of the system, results showed that the theoretical protocol can provide valuable insights into the interactions between an inorganic material and water pollutants, which can be useful for the design and optimization of inorganic materials for pollutant removal.

In [18] highlights the promising properties of  $\text{Al}_2\text{O}_3 \times 3\text{SiO}_2 \times \text{nH}_2\text{O}$  silicate-based material for the removal of metal ions from wastewater. However, the metal/adsorbent interaction was not theoretically supported. It would be interesting to study the usefulness of better understanding the interaction mechanisms between heavy metal ions and silicate-based adsorbents. In this sense, theoretical studies provide the foundation for understanding the interactions between heavy metals and silicate-based material, while experimental studies provide the empirical evidence needed to design silicate-based material with improved properties and refine the theoretical models. Furthermore, using this theoretical approach would significantly reduce the time and financial resources required for future experimental testing.

The research method adopted in this research involves a three-step process. First, using theoretical tools the interactions of metals adsorption onto the  $\text{Mg}_2\text{O}_8\text{Si}_3\text{M}$  ( $\text{M} = \text{Mn}^{2+}$ ,  $\text{Cu}^{2+}$ ,  $\text{Co}^{2+}$ ,  $\text{Zn}^{2+}$ ) clusters were identified. This was done by investigating the interaction between process variables and computing the conditions with fewer experiments. Second, the synthesis and characterization of hydrated amorphous magnesium silicate ( $\text{MgOSiO}_2 \times \text{nH}_2\text{O}$ ) material was developed. Last, a kinetic study of metal ion sorption ( $\text{Mn}^{2+}$ ,  $\text{Cu}^{2+}$ ,  $\text{Co}^{2+}$ ,  $\text{Zn}^{2+}$ ) using the synthetic  $\text{MgOSiO}_2 \times \text{nH}_2\text{O}$  was analyzed. This knowledge can then be used to design and optimize silicate-based materials for effective heavy metal removal, contributing to efforts to address environmental pollution and protect public health.

## 2. Material and methods

### 2.1. Molecular modelling

In this study, we systematically explored the Potential Energy Surface (PES) using a stochastic Kick method (*SnippetKick*, <https://github.com/HumanOsv/SnippetKick>) [36,37]. This method uses fragments (atoms or clusters) as building units of the system of interest. The fragments, centered at the origin of coordinates, are randomly rotated and repelled along random trajectories (Kick process) within a confinement space to avoid disconnected structures. We explored 1000 individuals, with 200 individuals per system,  $\text{Mg}_2\text{O}_8\text{Si}_3\text{M}$  ( $\text{M} = \text{Mn}^{2+}$ ,  $\text{Co}^{2+}$ ,  $\text{Cu}^{2+}$ , and  $\text{Zn}^{2+}$ ). For the screening, we considered the structure of the  $\text{Mg}_2\text{O}_8\text{Si}_3$  cluster (<https://pubchem.ncbi.nlm.nih.gov/compound/138394709>), combining them with the  $\text{Mn}^{2+}$ ,  $\text{Co}^{2+}$ ,  $\text{Cu}^{2+}$ , and  $\text{Zn}^{2+}$  metals. The initial screening was performed at the PBE0 [38]/SDDAll [39] level. Low-lying energy isomers ( $< 40.0$  kcal/mol above the putative global minimum) were re-minimized at the PBE0-D3 (BJ) [40]/def2-TZVP [41] level in the Gaussian16 package [42]. In our

analysis, the Wiberg bond index (WBI) was used to examine the strength and character of the bonds within the material or between the material and the adsorbed contaminants. It provides a numerical estimate of the bond order, with a WBI of 1 typically indicating a single bond, 2 a double bond, and so on [43]. To explore the charge transfer channel the Natural population analysis (NPA) [33] was performed with the natural bond orbital (NBO) code [44] (coupled to Gaussian package) Additionally, we performed the Independent Gradient Model based on Hirshfeld partition (IGMH) [32], with the Multiwfn v3.8 program [45] IGMH is a new method proposed for visually analyzing intramolecular and intermolecular interactions in chemical systems. It builds upon the existing Independent Gradient Model (IGM) method by replacing the free-state atomic densities used in IGM with atomic densities obtained from Hirshfeld partitioning of the molecular density. This gives IGMH a more rigorous physical basis. IGMH has advantages over other popular visualization methods like Non-covalent Interaction (NCI) plots. It can separately visualize intrafragment and interfragment interactions with smoother and less jagged isosurfaces. Furthermore, to analyze the weak interactions, present in the formation of the  $Mg_2O_8Si_3M$  ( $M = Mn^{2+}$ ,  $Co^{2+}$ ,  $Cu^{2+}$ , and  $Zn^{2+}$ ) clusters of the global minimum (GM) found in the exploration of PES, the Quantum Theory of Atoms in Molecules (QTAIM) developed by Bader [30,46,47], which is implemented in the Multiwfn v3.8 program, was employed. Through this methodology, it became possible to estimate a number of key topological properties, such as the Electron density ( $\rho$ ), Hamiltonian kinetic energy  $K(r)$ , Potential energy density  $V(r)$ , Total energy density  $H(r)$ , Laplacian of electron density ( $\nabla^2\rho$ ), Lagrangian kinetic energy  $G(r)$ , Ellipticity ( $\epsilon$ ),  $sign(\lambda^2)\rho$  provides information about the nature of interactions, and  $\delta_g$  function defined in IGMH partition. These properties were evaluated at the Bond Critical Points (BCPs).

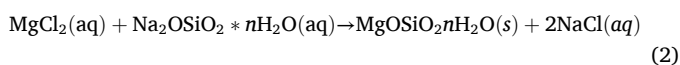
To determine the adsorption capacity of Magnesium Silicate ( $Mg_2O_8Si_3$ ) towards metal ions ( $M = Mn^{2+}$ ,  $Co^{2+}$ ,  $Cu^{2+}$ , and  $Zn^{2+}$ ) the adsorption energy ( $\Delta E_{ads}$ ) was calculated, which was estimated by the following Eq. (1) [48–50]:

$$\Delta E_{ads} = E_{Magnesium\ Silicate+M} - (E_{Magnesium\ Silicate} + E_M) \quad (1)$$

where,  $E_{Magnesium\ Silicate+M}$ ,  $E_{Magnesium\ Silicate}$  and  $E_M$  are the total energies with their respective zero-point energy (ZPE) corrections.

## 2.2. Synthesis of adsorbent

The  $MgOSiO_2nH_2O$  was synthesized using the sol-gel method previously reported in [18]. In brief, it was adding 1 L of  $MgCl_2$  (0.7 mol/l) to the sodium silicate ( $Na_2OSiO_2 \cdot nH_2O$ , 1.0 mol/l) and KOH to pH=14, avoiding precipitated silica and the magnesium hydroxide formation. Then, the solution was kept to 30 °C for 2 hrs. It was filtered and washed with distilled water. The product was dried in an oven at 80 °C for further grinding and sieving to obtain a particle between 0.125–0.200 mm. Eq. (2) represents the equation of the synthesis.



## 2.3. Characterization techniques

To identify functional groups, an FTIR model PV 9512 Phillips was used. Samples were conditioned in KBr (0.2 %) pellets. The data are reported in wavenumbers ( $cm^{-1}$ ). X-ray diffraction (XRD) measurement was made using a TUR-62 M unit with an HZG-3 diffractometer with  $CuK\alpha$  radiation ( $\lambda=1.5406 \text{ \AA}$ ). The samples were scanned between 4° and 75° For the ionic product (PI) determination was necessary to keep the  $MgOSiO_2nH_2O$  in contact for 24 h with a water solution. Then, using Eq. (3) and the atomic absorption spectroscopy technique the magnesium ( $Mg^{2+}$ ) amount in the solution was calculated. To determine the heat of dissociation ( $\Delta H_d$ ) in water, the Van't Hoff equation is used (see

Eq. (4)). Where C is a constant,  $\Delta H_d$  is the enthalpy change; (R is the universal gas constant (8.314 J/mol K), and T represents the absolute temperature (K). This equation shows that the natural logarithm of the ionic product is inversely proportional to the temperature. This means that as the temperature increases, the ionic product decreases and vice versa. The exact relationship depends on the enthalpy change of the reaction.

$$PI = aX \cdot a[Y]X = Mg^{2+}Y = [SiO_2(OH)_2]^{2-} \quad (3)$$

$$\ln PI = C - \frac{\Delta H_d}{RT} \quad (4)$$

To determine the mass loss to different media the  $MgOSiO_2nH_2O$  was placed in contact for 24 h with different aggressive media. The different aggressive media resistance such as corrosive, acidic, basic, and oxidizing agents is a significant aspect in the adsorbent materials characterization. It is possible to evaluate the conditions to be used without giving rise to chemical modification. The acid medium was evaluated through an HCl (ac) solution at 33 %, the basic medium was evaluated with NaOH (0.05 M), the corrosive medium was composed of a NaCl(ac) (0.01 M) solution and exposed to NaOCl (ac) at 10 % as an oxidizing agent. The physical characterization also included parameters such as the real density ( $d_{real}$ ), and apparent density ( $d_a$ ) shown in Eqs. (5)-6, respectively. Both parameters were calculated by the pycnometric method. In Eq. (5),  $m_s$  is the dust mass (g),  $V_{pic}$  defines the volume of the pycnometer (ml),  $m_{liq}$  represents the solvent mass (g) and  $d_{sol}$  denotes the solvent density (g/ml). The apparent density was calculated by the volume displacement of the synthesized compound [51]. Then, the apparent density and apparent bulk density by entrapment are used for determining compressibility, a property that powders must decrease the occupied volume by the external force action like vibration, pressure, or agitation.

$$d_{real} = \frac{m_s}{V_{pic} - m_{liq}d_{sol}} \quad (5)$$

$$d_a = \frac{\left[ \frac{\sum m_s}{\Pi} \right]}{V} \quad (6)$$

Porosity (P) is a roughness and capillarity measure of a given surface. The determination of this parameter can be complex, but a simple way is to link the porosity to the material density using Martin's equation [52] (Eq. (7)). Using a simple way to calculate the flow rate parameter, the Mohsenin equation was used [52,53]. Fick's first law was applied to obtain effective and theoretical diffusivity (see Table 1). Ten replicates were done in all cases.

$$P = 1 - \left[ \frac{d_a}{d_{real}} \right] * 100 \quad (7)$$

The specific surface area (S) is also a significant property in the sorbent materials characterization. In this sense, S was determined by

**Table 1**  
Parameters calculated in the chemical and physical analysis.

Effective and theoretical diffusivity	Tortuosity ( $\gamma/cm^3$ )	Mean pore volume ( $cm^3$ )	Mean pore radius (cm)	Hollow Fraction	Surface area ( $m^2/g$ )
$D_{ef} = \frac{D_T \cdot d_a}{\gamma}$	$\gamma = 2 - d_a$	$r_m = \frac{2V_p}{S}$	$r_m = \frac{2P}{Sd_r}$	$F_h = \frac{V_p}{V_p + 1d_r}$	$S = \frac{q_e N A_m}{10^{-20}}$

apparent density ( $d_a$ ) tortuosity ( $\gamma$ ), theoretical diffusivity ( $D_T$ ), effective diffusivity ( $D_{ef}$ ), S is the specific surface area ( $m^2/g$ ),  $q_e$ , the number of milligrams absorbed per gram of solvent ( $mg\ g^{-1}$ ),  $A_m$ , the surface area of the methylene blue ( $\text{\AA}$ ) and the monolayer mass (g).

the dye methylene blue (MB:  $C_{16}H_{18}N_3SCl$ ) method [54]. Before this, a kinetic study was carried out to determine the compound's maximum sorption time. This study was carried out by placing the methylene blue (15 mg/L) in contact with 0.10 g of the material, previously dried at 200 °C. The absorbance values were determined at 660 nm, at intervals of 2 min using a spectrophotometer Shimadzu UV-1900. After establishing the maximum adsorption time, a thermodynamic study (Langmuir model) was carried out based on methylene blue samples of known concentration (0.6, 1.2, 1.5, 1.8, 2.4, 3.0, 4.5, 7.5, 10.5, and 15.0 mg/L) were placed in contact with 0.10 g of  $MgOSiO_2 \cdot nH_2O$  for 1 hour. Langmuir's model considered that adsorption occurs homogeneously over the entire surface, making it possible to determine the monolayer mass and the specific surface using the last equation shown in Table 1. The MB surface area was determined by molecular descriptors, using the Dragon program [55]. The area corresponding to the complete molecule ( $C_{16}H_{18}N_3SCl$ ) was 507.2 Å. The MB method can determine important parameters like pore volume ( $V_p$ ), pore radius ( $r_m$ ), and the hollow fraction ( $F_h$ ). Furthermore, the apparent ion exchange capacity was estimated by taking a small amount of  $MgOSiO_2 \cdot nH_2O$  and placing it in contact with the KCl solution over time, taking the values of the initial ( $C_i$ ) and concentration at time ( $C_e$ ) in mg/L.

#### 2.4. Kinetic study of metals adsorption

To determine the initial concentration effect of each metal ion and the time required to achieve adsorption equilibrium the kinetics adsorption process was investigated. First, the sorbent mass was optimized and submitted to physical activation at 200 °C before contacting the ions to eliminate adsorbed water molecules on the surface. Each sample was subjected to individual metal exposure. Several kinetic parameters are calculated, such as adsorbate adsorbed per gram of the adsorbent at equilibrium ( $q_e$ ), total lifetime (t), and media lifetime ( $t_{1/2}$ ). A known concentration solution of the metal ions was set in contact with  $MgOSiO_2 \cdot nH_2O$  at 500 rpm. Table 2 shows the concentration, product mass, and maximum sorption time values used in the kinetic analysis. The concentrations were selected to have excess metal ions in the solution concerning the material absorption capacity to achieve full saturation and ensure its maximum sorption capacity.

The initial ( $C_i$ ) and breakeven (maximum absorption) ( $C_e$ ) metal concentrations were determined at different time intervals using the atomic absorption spectroscopy method using PYE UNICAM SP9 (U.K.). These analyses were contracted to an accredited laboratory of the Center for Agricultural Research (CIAP), Universidad Central "Marta Abreu de las Villas", Cuba. The kinetic models' analysis was done using a simple linear regression method of least squares with Origin statistical package version 10.0.5.157 (Academic). To check the kinetic model's validity the determination coefficient ( $R^2$ ) was used.  $R^2$  close to 1 indicates the more efficient models. Table 3 shows the kinetic models evaluated.

#### 2.5. Statistical procedure

The characterization data were processed statistically using the Kolmogorov–Smirnov and Bartlett tests to verify normality and homogeneity of variance (10 replicates for each sample analyzed). The correlation analyses were conducted using the Pearson simple linear correlation matrix and the Spearman rank correlation test both for a

**Table 2**  
Concentration, product mass, and maximum sorption time values obtained in the kinetic analysis.

Metals ions	Initial concentration ( $C_i$ , g/L)	Absorbent mass (g)	Time (min)
Mn <sup>2+</sup>	0.598	0.1	29
Co <sup>2+</sup>	0.960	0.1	32
Cu <sup>2+</sup>	0.950	0.1	55
Zn <sup>2+</sup>	0.592	0.1	58

**Table 3**  
Kinetic models employed in heavy metal adsorption.

Models	Equations	Variable Descriptor
Pseudo First Order [56]	$\ln(q_e - q_t) = \ln(q_e - k_1 t)$ $t_{1/2} = \frac{\ln 2}{k_1}$	Dependence between $\ln(q_e - q_t)$ vs t where $q_e$ is the amount in grams of solute adsorbed per gram of adsorbent at equilibrium (mg g <sup>-1</sup> ); $q_t$ represents the grams of solute adsorbed per gram of adsorbent over time (mg g <sup>-1</sup> ); t is the time in min, $k_1$ is the pseudo first order adsorption rate constant (min <sup>-1</sup> ) and $t_{1/2}$ is the mean lifetime in min.
Pseudo Second Order [57]	$\frac{1}{q_t} = \frac{1}{k_2 q_e^2}$ $t_{1/2} = \frac{1}{q_e k_2}$ $h_2 = k_2 q_e$	Dependence between $1/q_t$ vs t, where $q_e$ is the amount in grams of solute adsorbed per gram of adsorbent at equilibrium (mg g <sup>-1</sup> ); $q_t$ represents the grams of solute adsorbed per gram of adsorbent over time (mg g <sup>-1</sup> ); $h_2$ is the initial absorption rate (mg g <sup>-1</sup> min); $t_{1/2}$ represents the mean lifetime in min, and $k_2$ is the initial rate constant.
Intraparticle Diffusion [58]	$q_t = kt^{1/2} + C$	Dependence between $q_t$ vs t, where $q_t$ is the amount of solute adsorbed per gram of adsorbent over time (mg g <sup>-1</sup> ); $t_{1/2}$ represents the time variable in min; k is the intraparticle diffusion rate constant and C is a constant.
Elovich Model [19]	$q_t = \alpha + \beta \ln t$	Dependence between $q_t$ vs $\ln t$ , where $q_t$ represents the milligrams of solute adsorbed per gram of adsorbent over time (mg g <sup>-1</sup> ); $\alpha$ is the initial sorption rate (mg/min); $\beta$ is the sorption constant (mg/min) and t is the time in min.

reliability level of 95 %. All these statistical tests are included in the R statistical package [59] version 3.6.2.

### 3. Results and discussion

This section shows the main results of the metal/silicate-based adsorbent interactions from the theoretical and experimental analysis. We proceed with the molecular modeling of  $Mg_2O_8Si_3M$  ( $M = Mn^{2+}$ ,  $Co^{2+}$ ,  $Cu^{2+}$ , and  $Zn^{2+}$ ) clusters and the synthesis and chemical-physical characterization of  $MgOSiO_2 \cdot nH_2O$  material. Once the characteristics of the material and the conditions under which it could be used were established, a simple kinetic test was performed. The above to validate the theoretical predictions results and provide practical information that can be used in wastewater remediation and the design of new silicate-based materials with better properties. Lastly, future perspectives of this research are highlighted to emphasize the need to show interest in more experimental techniques for a deeper analysis of  $MgOSiO_2 \cdot nH_2O$  and the removal of heavy metals.

#### 3.1. Molecular modelling

We have performed a comprehensive potential energy surface (PES) analysis of  $Mg_2O_8Si_3M$  ( $M = Mn^{2+}$ ,  $Co^{2+}$ ,  $Cu^{2+}$ , and  $Zn^{2+}$ ) clusters, meticulously following the protocol detailed in the computational methods section. This approach has allowed us to explore a wide range of structures and identify energetically more stable ones. Our results reveal a preference for metal atoms ( $Mn^{2+}$ ,  $Cu^{2+}$ ,  $Co^{2+}$ ,  $Zn^{2+}$ ) to position themselves close to the oxygen atoms in the Magnesium Silicate, which contributes significantly to the stabilization of the  $Mg_2O_8Si_3M$  systems, as illustrated in Fig. 1. Importantly, the clusters in this figure correspond to the putative global minimum in the PES, while additional isomers are presented in Figs. S1–S4. For each  $Mg_2O_8Si_3$  cluster, we observe a variation in the coordination number of the metal atoms with the oxygen atoms of  $Mg_2O_8Si_3$ . For example, in the  $Mg_2O_8Si_3Mn$  cluster, the Mn atom exhibits coordination with four central oxygen atoms of the  $Mg_2O_8Si_3$  cluster, whereas for the  $Mg_2O_8Si_3Cu$  and  $Mg_2O_8Si_3Co$  clusters, the Cu and Co atoms show coordination with two central oxygen atoms

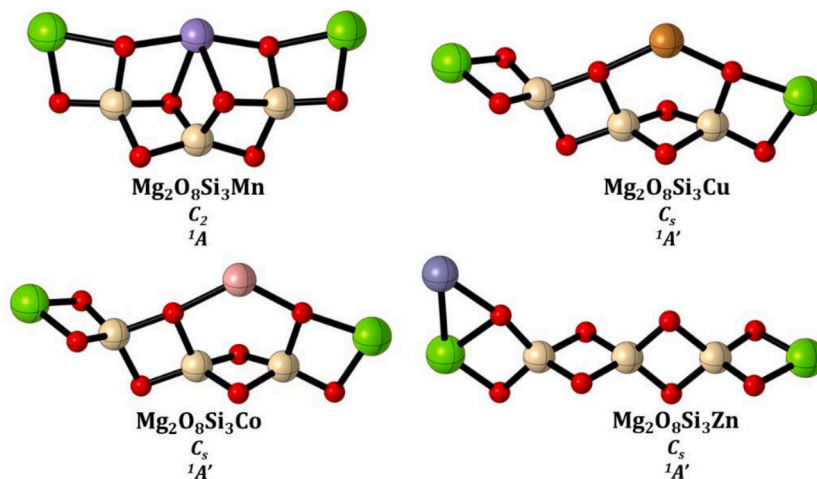


**Fig. 1.** Lower energy structures of  $\text{Mg}_2\text{O}_8\text{Si}_3\text{M}$  ( $\text{M} = \text{Mn}^{2+}, \text{Cu}^{2+}, \text{Co}^{2+}, \text{Zn}^{2+}$ ) clusters at the PBE0-D3(BJ)/Def2-TZVP level. Color coding for spheres: red = oxygen, yellow = silicon, green = magnesium, purple = manganese, orange = copper, pink = cobalt, and ice blue = zinc.

of the  $\text{Mg}_2\text{O}_8\text{Si}_3$  cluster. Finally, in the  $\text{Mg}_2\text{O}_8\text{Si}_3\text{Zn}$  cluster, the Zn atom coordinates with an oxygen atom at the end of the  $\text{Mg}_2\text{O}_8\text{Si}_3$  cluster, accompanied by an interaction with a magnesium atom of the  $\text{Mg}_2\text{O}_8\text{Si}_3$  cluster.

The adsorption of metallic ions ( $\text{Mn}^{2+}, \text{Co}^{2+}, \text{Cu}^{2+},$  and  $\text{Zn}^{2+}$ ) on the  $\text{Mg}_2\text{O}_8\text{Si}_3$  cluster was analyzed by determining the adsorption energy as  $\Delta E_{\text{ads}} = E_{\text{Magnesium Silicate}+\text{M}} - (E_{\text{Magnesium Silicate}} + E_{\text{M}})$ . This  $\Delta E_{\text{ads}}$  was examined for the  $\text{Mg}_2\text{O}_8\text{Si}_3\text{M}$  ( $\text{M}$  representing  $\text{Mn}^{2+}, \text{Cu}^{2+}, \text{Co}^{2+}, \text{Zn}^{2+}$ ) clusters, as illustrated in Fig. 1. According to this approach, a more negative adsorption energy value indicates a more energy-efficient adsorption process and suggests stronger interactions [48,49]. Table 4 displays all  $\Delta E_{\text{ads}}$ , as can be seen, all values for these energies were negative, thus the adsorption of this metal on the surface of the  $\text{Mg}_2\text{O}_8\text{Si}_3$  cluster is energetically favorable.

In all systems of  $\text{Mg}_2\text{O}_8\text{Si}_3$  with the heavy metals  $\text{Mn}^{2+}, \text{Cu}^{2+}, \text{Co}^{2+}$  and  $\text{Zn}^{2+}$ , a negative  $\Delta E_{\text{ads}}$  is observed. This means that the adsorption is thermodynamically favorable for all these metals, suggesting a strong interaction between the metal cations and the material structure, favoring the stability of the system. Among all the systems examined, the  $\text{Mg}_2\text{O}_8\text{Si}_3\text{Mn}$  system stood out remarkably in terms of the  $\Delta E_{\text{ads}}$ , with a value of  $-5.8$  eV, indicating a strong interaction. This result is attributed to the coordination of the Mn atom with the four oxygen atoms of the  $\text{Mg}_2\text{O}_8\text{Si}_3$  cluster, suggesting the formation of a stable coordination site for the Mn atom. In contrast, the  $\text{Mg}_2\text{O}_8\text{Si}_3\text{Cu}$  and  $\text{Mg}_2\text{O}_8\text{Si}_3\text{Co}$  systems exhibited lower  $\Delta E_{\text{ads}}$  values, with minimal differences between them of  $-2.4$  and  $-3.1$  eV, respectively, compared to the  $\text{Mg}_2\text{O}_8\text{Si}_3\text{Mn}$  system. On the other hand, the  $\text{Mg}_2\text{O}_8\text{Si}_3\text{Zn}$  system showed the lowest  $\Delta E_{\text{ads}}$  value, with  $-1.1$  eV. These discrepancies between the systems suggest an energetically more favourable state for the  $\text{Mg}_2\text{O}_8\text{Si}_3\text{Mn}$  system, which highlights its thermodynamic stability in contrast to the interactions with  $\text{Cu}^{2+}, \text{Co}^{2+}, \text{Zn}^{2+}$  atoms. In general, it is observed that as the coordination between the oxygen atoms of  $\text{Mg}_2\text{O}_8\text{Si}_3$  and the heavy metals ( $\text{Mn}^{2+}, \text{Cu}^{2+}, \text{Co}^{2+}, \text{Zn}^{2+}$ ) increases, the value of  $\Delta E_{\text{ads}}$  indicates a differential energetic preference between the systems, highlighting the influence of configuration and coordination on the stability of the complexes formed.

A detailed analysis of the bond distances between heavy metal and oxygen atoms (M-O) for the  $\text{Mg}_2\text{O}_8\text{Si}_3\text{M}$  ( $\text{M} = \text{Mn}^{2+}, \text{Cu}^{2+}, \text{Co}^{2+}, \text{Zn}^{2+}$ ) clusters is presented in Table 4. Notably, the  $r_{\text{M-O}}$  distances for the  $\text{Mg}_2\text{O}_8\text{Si}_3\text{Mn}$  system are slightly larger, ranging between 1.96 and 2.22 Å. Examining the  $\text{WBI}_{\text{M-O}}$  charge density values, which vary between 0.03 and 0.43, suggests that the nature of the covalent M-O interaction is relatively weak, suggesting a possible more ionic behavior [60]. On the other hand, the  $\text{WBI}_{\text{M-O}}$  values observed for the  $\text{Mg}_2\text{O}_8\text{Si}_3\text{Mn}$  system fall

**Table 4**

Bond lengths ( $r$ , Å), Wiberg bond indices (WBI), NPA charges ( $q$ ,  $|e|$ ) and  $\Delta E_{\text{ads}}$  (eV) of the  $\text{Mg}_2\text{O}_8\text{Si}_3\text{M}$  ( $\text{M} = \text{Mn}, \text{Cu}, \text{Co}, \text{Zn}$ ) clusters calculated at PBE0-D3(BJ)/Def2-TZVP level.

System	$r_{\text{M-O}}$	$\text{WBI}_{\text{M-O}}$	$q$ (M)	$q(\text{O})$	$q(\text{Mg})$	$\Delta E_{\text{ads}}$
$\text{Mg}_2\text{O}_8\text{Si}_3\text{Mn}$	1.96 -	0.19 -	2.06	-0.58 -	0.02	-5.8
	2.22	0.43		-0.69		
$\text{Mg}_2\text{O}_8\text{Si}_3\text{Cu}$	1.93 -	0.03 -	0.41	-0.59 -	0.91 -	-2.4
	2.00	0.05		-0.71		
$\text{Mg}_2\text{O}_8\text{Si}_3\text{Co}$	1.93 -	0.05 -	0.42	-0.59 -	0.91 -	-3.1
	2.00	0.07		-0.71		
$\text{Mg}_2\text{O}_8\text{Si}_3\text{Zn}$	2.02	0.15	0.25	-1.20 -	1.58 -	-1.1
				-1.50		

within the range of 0.19 to 0.43, indicating a more intense interaction compared to the other systems. These values closely align with the characteristic ionic interaction patterns and complement the strong interaction of the four oxygen atoms with the Mn atom in this system.

A detailed analysis of the NPA charge distribution reveals a charge transfer from the heavy atom M to the  $\text{Mg}_2\text{O}_8\text{Si}_3$  cluster. This charge transfer, quantified by the parameter  $q(\text{M})$ , exhibits a significant variation, ranging from 0.25 to 2.06  $|e|$ , and a gradual increase from  $\text{Zn}^{2+}$  to  $\text{Mn}^{2+}$  is observed, see Table 4 and Fig. 2, top image. This phenomenon highlights the tendency of heavy metals to lose electrons and acquire a cationic character in the presence of the  $\text{Mg}_2\text{O}_8\text{Si}_3$  cluster, with  $\text{Mn}^{2+}$  showing the highest charge transfer. This observation is consistent with the electropositive nature of  $\text{Mn}^{2+}$ , characterized by its tendency to give up electrons in chemical interactions, resulting in the formation of stable cations [61].

The interaction of heavy metal atoms with oxygen in the  $\text{Mg}_2\text{O}_8\text{Si}_3\text{M}$  ( $\text{M} = \text{Mn}^{2+}, \text{Cu}^{2+}, \text{Co}^{2+}, \text{Zn}^{2+}$ ) systems exhibits a strong ionic character, as evidenced by the Independent Gradient Model based on Hirshfeld partition (IGMH) analysis. Fig. 2, bottom image, illustrates the nature of these interactions, where the blue isosurfaces represent the regions of strong ionic bonding. In the  $\text{Mg}_2\text{O}_8\text{Si}_3\text{Mn}$  system, the Mn atom forms a coordination with four oxygen atoms of the  $\text{Mg}_2\text{O}_8\text{Si}_3$  framework. This coordination environment suggests a tetrahedral geometry around the Mn center, facilitated by the ionic interactions with the surrounding oxygen atoms. The  $\text{Cu}^{2+}$  in the  $\text{Mg}_2\text{O}_8\text{Si}_3\text{Cu}$  system coordinates with two oxygen atoms of the  $\text{Mg}_2\text{O}_8\text{Si}_3$  framework, forming a linear geometry. The reduced coordination number compared to Mn indicates a weaker ionic interaction strength for  $\text{Cu}^{2+}$ . Similarly, the  $\text{Co}^{2+}$  atom in the  $\text{Mg}_2\text{O}_8\text{Si}_3\text{Co}$  system also coordinates with two oxygen atoms of the  $\text{Mg}_2\text{O}_8\text{Si}_3$  framework, adopting a linear geometry. This coordination

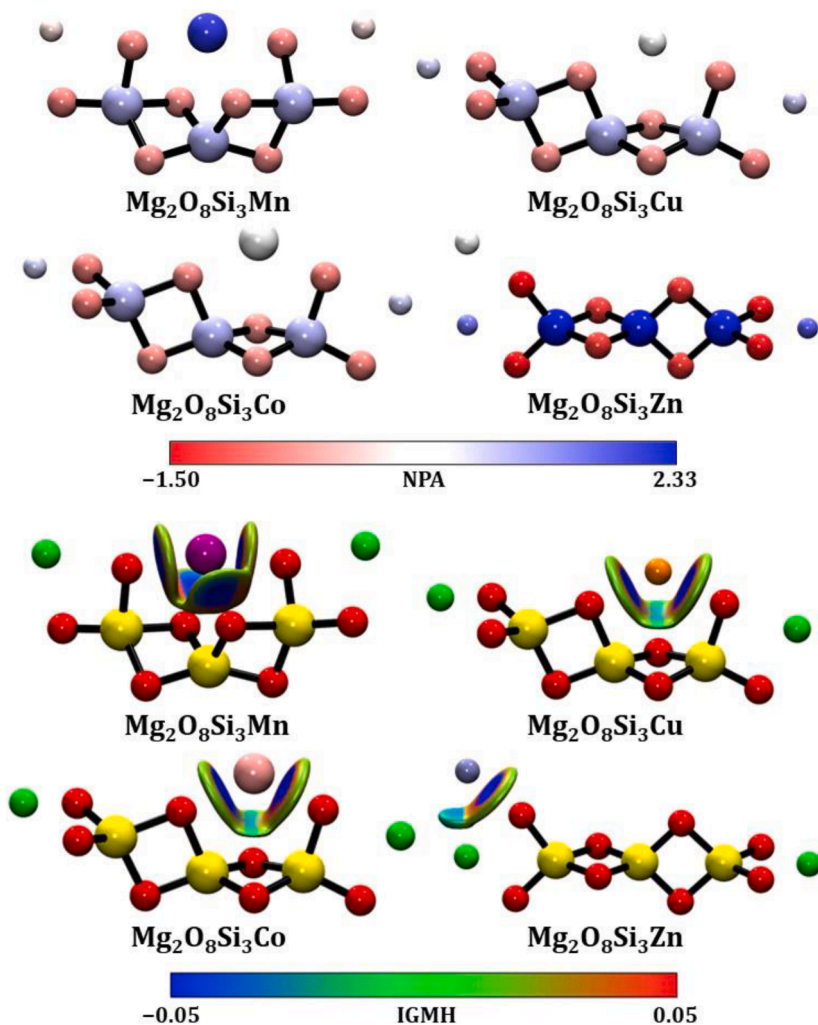


**Fig. 2.** (Top) NPA charge values and (Bottom) IGMH analysis ( $\delta g^{\text{inter}}=0.003$  a.u.) for  $\text{Mg}_2\text{O}_8\text{Si}_3\text{M}$  ( $M = \text{Mn}^{2+}, \text{Cu}^{2+}, \text{Co}^{2+}, \text{Zn}^{2+}$ ) clusters. The prominent strong attractive interaction zone, specifically the oxide-metal bond, these bonds have a more ionic character due to the higher electronegativity difference between the metal and oxygen, which is depicted by the blue isosurface. Color coding for spheres: red = oxygen, yellow = silicon, green = magnesium, purple = manganese, orange = copper, pink = cobalt, and ice blue = zinc.

environment suggests a comparable ionic interaction strength to that observed in the Co system. In contrast, the  $\text{Zn}^{2+}$  in the  $\text{Mg}_2\text{O}_8\text{Si}_3\text{Zn}$  system exhibits the weakest ionic interaction, coordinating with only

one oxygen and magnesium atom of the  $\text{Mg}_2\text{O}_8\text{Si}_3$  framework. This reduced coordination number implies a weaker ionic bonding character for Zn compared to the other heavy metal systems studied.

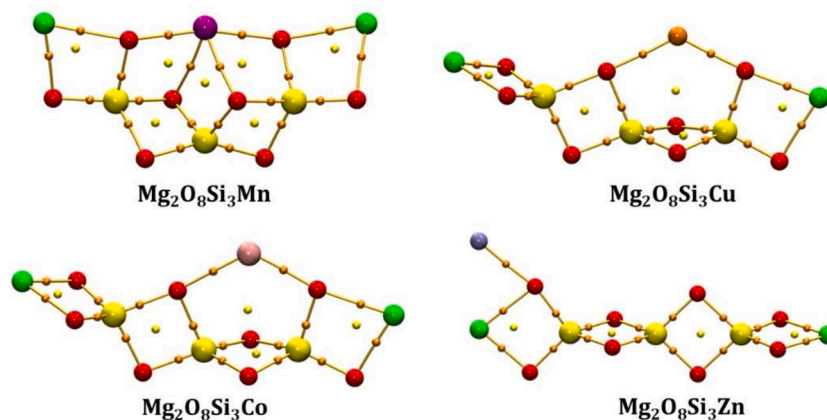


**Fig. 3.** AIM molecular graph showing the different Bond Critical Points (BCPs) of  $\text{Mg}_2\text{O}_8\text{Si}_3\text{M}$  ( $M = \text{Mn}^{2+}, \text{Cu}^{2+}, \text{Co}^{2+}, \text{Zn}^{2+}$ ) clusters. Yellow and orange small spheres in the above map correspond to  $(3,+1)$  and  $(3,-1)$  critical points, respectively. Brown lines denote bond paths. Color coding for big spheres: red = oxygen, yellow = silicon, green = magnesium, purple = manganese, orange = copper, pink = cobalt, and ice blue = zinc.

The QTAIM analysis provides valuable insights into the electron density distribution and bonding characteristics of the  $\text{Mg}_2\text{O}_8\text{Si}_3\text{M}$  ( $\text{M} = \text{Mn}^{2+}, \text{Cu}^{2+}, \text{Co}^{2+}, \text{Zn}^{2+}$ ) systems. Fig. 3 illustrates the topology of the electron density, highlighting the positions of bond critical points (BCPs) denoted by coordinates such as (3,+1) and (3,-1), which represent saddle points and bond paths connecting different molecular components. In the  $\text{Mg}_2\text{O}_8\text{Si}_3\text{Mn}$  system, four (3,-1) BCPs are observed, indicating the formation of four bonding interactions involving the Mn atom. Additionally, three (3,+1) BCPs are present, suggesting the existence of ring structures within the molecular framework. In the case of  $\text{Mg}_2\text{O}_8\text{Si}_3\text{Cu}$  and  $\text{Mg}_2\text{O}_8\text{Si}_3\text{Co}$  systems exhibit two (3,-1) BCPs, indicating the formation of two bonding interactions involving the  $\text{Cu}^{2+}$  and  $\text{Co}^{2+}$ , respectively. Furthermore, a single (3,+1) BCP is observed in each system, suggesting the presence of a ring structure within the molecular framework. The  $\text{Mg}_2\text{O}_8\text{Si}_3\text{Zn}$  system displays a single (3,-1) BCP, indicating the formation of one bonding interaction involving the Zn atom.

The analysis of bonding critical points (BCPs) using topological methods in the  $\text{Mg}_2\text{O}_8\text{Si}_3\text{M}$  ( $\text{M} = \text{Mn}^{2+}, \text{Cu}^{2+}, \text{Co}^{2+}, \text{Zn}^{2+}$ ) clusters offers profound insights into the intricate nature of interactions between heavy metal atoms and surrounding oxygen atoms. Table 5, meticulously presents crucial topological parameters characterizing these BCPs, encompassing electron density ( $\rho$ ), Hamiltonian kinetic energy  $K(r)$ , potential energy density  $V(r)$ , total energy density  $H(r)$ , Laplacian of electron density  $\nabla^2\rho$ , Lagrangian kinetic energy  $G(r)$ , ellipticity ( $\epsilon$ ), sign( $\lambda_2$ ) $\rho$ , and the  $\delta_g$  function, as defined in the IGMH partition. In the  $\text{Mg}_2\text{O}_8\text{Si}_3\text{Mn}$  system, the Mn atom engages in four Mn–O bonds, a fact substantiated by the presence of four BCPs. The relatively elevated electron density ( $\rho \approx 0.09$ ) and positive Laplacian values ( $\nabla^2\rho \approx 0.45$ ) at these BCPs point towards a notable ionic character in these bonding interactions. Nonetheless, the negative total energy density  $H(r)$  values hint at a degree of covalency, a notion further supported by intermediate  $\delta_g$  values ( $\approx 0.2$ ). Meanwhile, in the  $\text{Mg}_2\text{O}_8\text{Si}_3\text{Cu}$  system, two O–Cu bonds are discerned, characterized by BCPs exhibiting high electron density ( $\rho \approx 0.09$ ) and positive Laplacian values ( $\nabla^2\rho \approx 0.47$ ), indicative of robust ionic interactions. Yet again, negative  $H(r)$  values alongside intermediate  $\delta_g$  values ( $\approx 0.2$ ) suggest some degree of covalency. Similarly, the  $\text{Mg}_2\text{O}_8\text{Si}_3\text{Co}$  system showcases two O–Co bonds with relatively high electron density ( $\rho \approx 0.08$ ) and positive Laplacian values ( $\nabla^2\rho \approx 0.44$ ), implying substantial ionic character. The negative  $H(r)$  values and intermediate  $\delta_g$  values ( $\approx 0.2$ ) further imply a covalent component in these bonds, akin to the  $\text{Cu}^{2+}$  system. In addition, in the  $\text{Mg}_2\text{O}_8\text{Si}_3\text{Zn}$  system, a single Zn–O bond is evident, characterized by relatively high electron density ( $\rho \approx 0.07$ ) and a positive Laplacian value ( $\nabla^2\rho \approx 0.38$ ), indicative of a robust ionic interaction. Negative  $H(r)$  values alongside intermediate  $\delta_g$  values ( $\approx 0.16$ ) suggest a degree of covalency in this bond, albeit slightly lower compared to other systems.

**Table 5**

Topological analysis of the bonding critical points (BCP) of the  $\text{Mg}_2\text{O}_8\text{Si}_3\text{M}$  ( $\text{M} = \text{Mn}^{2+}, \text{Cu}^{2+}, \text{Co}^{2+}, \text{Zn}^{2+}$ ) clusters. Electron density ( $\rho$ ), Hamiltonian kinetic energy  $K(r)$ , Potential energy density  $V(r)$ , Total energy density  $H(r)$ , Laplacian of electron density ( $\nabla^2\rho$ ), Lagrangian kinetic energy  $G(r)$ , Ellipticity ( $\epsilon$ ), sign( $\lambda_2$ ) $\rho$ , and  $\delta_g$  function. All values are given in atomic units (a.u.).

Bonds	$\rho$	$K(r)$	$V(r)$	$H(r)$	$\nabla^2\rho$	$G(r)$	$\epsilon$	sign( $\lambda_2$ ) $\rho$	$\delta_g$
<b><math>\text{Mg}_2\text{O}_8\text{Si}_3\text{Mn}</math></b>									
Mn–O	$8.88 \times 10^{-2}$	$1.21 \times 10^{-2}$	$-1.36 \times 10^{-1}$	$-1.21 \times 10^{-2}$	$4.48 \times 10^{-1}$	$1.24 \times 10^{-1}$	$5.93 \times 10^{-2}$	$-8.88 \times 10^{-2}$	$2.17 \times 10^{-1}$
Mn–O	$8.88 \times 10^{-2}$	$1.20 \times 10^{-2}$	$-1.37 \times 10^{-1}$	$-1.20 \times 10^{-2}$	$4.51 \times 10^{-1}$	$1.25 \times 10^{-1}$	$4.93 \times 10^{-2}$	$-8.88 \times 10^{-2}$	$2.17 \times 10^{-1}$
Mn–O	$4.98 \times 10^{-2}$	$6.98 \times 10^{-3}$	$-6.84 \times 10^{-2}$	$-6.98 \times 10^{-3}$	$2.18 \times 10^{-1}$	$6.14 \times 10^{-2}$	$4.40 \times 10^{-1}$	$-4.98 \times 10^{-2}$	$1.06 \times 10^{-1}$
Mn–O	$5.06 \times 10^{-2}$	$7.24 \times 10^{-3}$	$-7.00 \times 10^{-2}$	$-7.24 \times 10^{-3}$	$2.22 \times 10^{-1}$	$6.28 \times 10^{-2}$	$4.24 \times 10^{-1}$	$-5.06 \times 10^{-2}$	$1.08 \times 10^{-1}$
<b><math>\text{Mg}_2\text{O}_8\text{Si}_3\text{Cu}</math></b>									
O–Cu	$9.28 \times 10^{-2}$	$2.56 \times 10^{-2}$	$-1.69 \times 10^{-1}$	$-2.56 \times 10^{-2}$	$4.71 \times 10^{-1}$	$1.44 \times 10^{-1}$	$2.73 \times 10^{-2}$	$-9.28 \times 10^{-2}$	$2.44 \times 10^{-1}$
O–Cu	$7.34 \times 10^{-2}$	$1.48 \times 10^{-2}$	$-1.28 \times 10^{-1}$	$-1.48 \times 10^{-2}$	$3.94 \times 10^{-1}$	$1.13 \times 10^{-1}$	$2.92 \times 10^{-2}$	$-7.34 \times 10^{-2}$	$1.88 \times 10^{-1}$
<b><math>\text{Mg}_2\text{O}_8\text{Si}_3\text{Co}</math></b>									
O–Co	$6.79 \times 10^{-2}$	$1.00 \times 10^{-2}$	$-1.16 \times 10^{-1}$	$-1.00 \times 10^{-2}$	$3.86 \times 10^{-1}$	$1.06 \times 10^{-1}$	$1.53 \times 10^{-1}$	$-6.79 \times 10^{-2}$	$1.60 \times 10^{-1}$
O–Co	$9.33 \times 10^{-2}$	$2.14 \times 10^{-2}$	$-1.63 \times 10^{-1}$	$-2.14 \times 10^{-2}$	$4.79 \times 10^{-1}$	$1.41 \times 10^{-1}$	$1.33 \times 10^{-1}$	$-9.33 \times 10^{-2}$	$2.34 \times 10^{-1}$
<b><math>\text{Mg}_2\text{O}_8\text{Si}_3\text{Zn}</math></b>									
Zn–O	$7.01 \times 10^{-2}$	$8.05 \times 10^{-3}$	$-1.10 \times 10^{-1}$	$-8.05 \times 10^{-3}$	$3.77 \times 10^{-1}$	$1.02 \times 10^{-1}$	$7.84 \times 10^{-2}$	$-7.01 \times 10^{-2}$	$1.64 \times 10^{-1}$

### 3.2. Characterization of adsorbent

The synthesis revealed that  $\text{MgOSiO}_2\text{nH}_2\text{O}$  displays a mass of  $300.13 \text{ g mol}^{-1}$ , which corresponds to MgO (35.40 %), to  $\text{SiO}_2$  (54.28 %), to  $\text{H}_2\text{O}$  (9.23 %), to  $\text{Na}_2\text{O}$  (0.15 %) and  $\text{Fe}_2\text{O}_3$  (0.91 %). Fig. 4a and b show the infrared spectra and powder X-ray diffraction (XRD) patterns, respectively. Generally, the FTIR spectra of the sample show bands between  $500$  and  $1106.42 \text{ cm}^{-1}$ . In this case, the IR spectrum analysis has confirmed the presence of bands characteristic of metal silicates in the  $514\text{--}1480 \text{ cm}^{-1}$  zone. These bands correspond to the different types of internal oscillations within the network, specifically those involving O–Si–O [62]. Silicates characteristic peaks in  $559.33, 742.43, 990.95,$  and  $1106.42 \text{ cm}^{-1}$  were found, which refer to the different types of internal oscillations within the network. The bands of  $1787.04 \text{ cm}^{-1}$  and  $3447.16 \text{ cm}^{-1}$  are attributed to the structural water (O–H) [63]. The XRD revealed that the  $\text{MgOSiO}_2\text{nH}_2\text{O}$  syntheses have an amorphous nature in one phase. It shows only a diffuse curve, indicating the crystallographic plane's absence with the same broad humps at  $19.7^\circ$  and  $26.7^\circ 2\theta$  as reported earlier for magnesium silicate hydrated [64].

On the other hand, Fig. 5 shows the enthalpy of the dissociation process calculated using the relationship between the ionic product ( $PI$ ) and the temperatures of  $293 \text{ K}, 303 \text{ K}, 313 \text{ K},$  and  $323 \text{ K}$ . According to this parameter (equal to  $-0.30 \text{ kJ/mol}$ ), the dissociation of material was exothermic. Therefore, the process will be favored at low temperatures; so, its use at low temperatures is not recommended. Results agree with other silicic materials reported [17,18].

The physical-chemical characterization of the sample was carried out trying to expose those more general properties of interest for the adsorbent materials. The material resistance is an important factor for its subsequent use. Table 6 shows the result of several physical parameters and the mass variations in the material after contact with different media over 24 h. The  $\text{MgOSiO}_2\text{nH}_2\text{O}$  displayed moderate resistance to acidic, basic, oxidizing, and corrosive media. This result suggests that this material can be used as an adsorbent in an aqueous matrix with a neutral pH. On the other hand, several physical parameters were determined to characterize the material (Table 6). The  $\text{MgOSiO}_2\text{nH}_2\text{O}$  displayed a low density, with a high porosity (87.67 %), which a considered adsorbing power, about 62.56 % can compress this compound, with zero flow rate giving the material a strong adhesion power. This latter characteristic gives an added value since it is a high surface area material, charged and very porous. Also, this material shows a high apparent ion exchange capacity, reaching 86.20 %. The values obtained for effective and theoretical diffusivity and tortuosity were found to be within the range of porous solids. From the MB method, the specific surface area of  $\text{MgOSiO}_2\text{nH}_2\text{O}$  was  $124.88 \text{ m}^2 \text{ g}^{-1}$ . The results fitted the Langmuir model ( $R^2=0.96$ ), which determined the maximum adsorption capacity of MB corresponding at  $q_e=4.44 \times 10^{-5} \text{ mol g}^{-1}$  sorbent. According to the pore volume, pore radius, hollow fraction, and specific

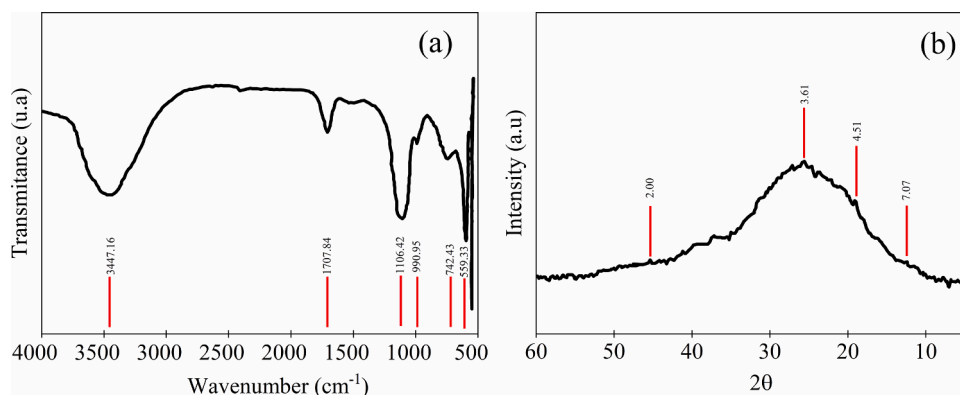


Fig. 4. (a) FTIR spectra and (b) X-ray diffraction of the synthetic magnesium silicate material.

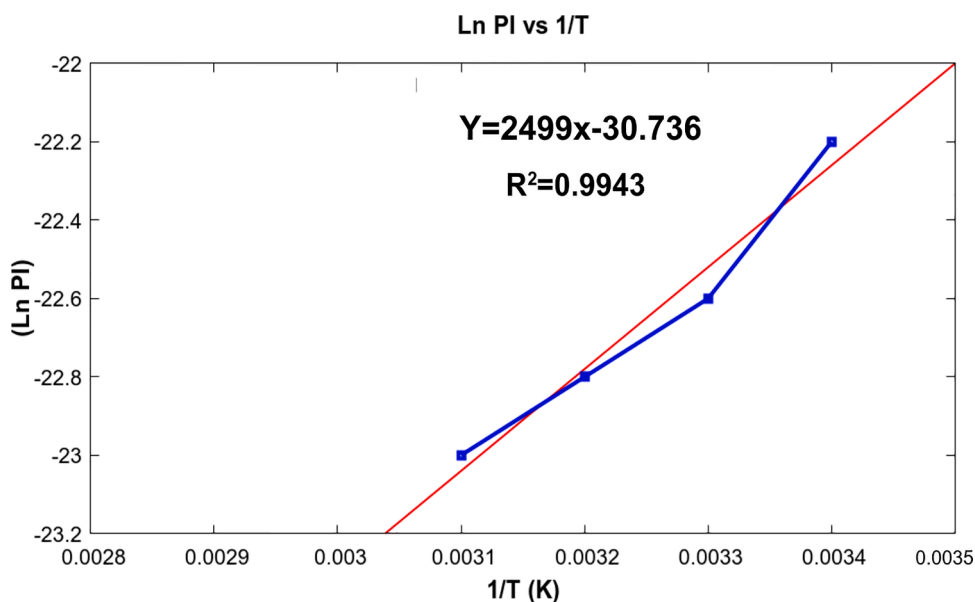


Fig. 5. Relationship between ionic product ( $\ln PI$ ) and temperature ( $T$ ) in Kelvin.

Table 6

Results of physical parameters obtained from laboratory experiments and chemical performance under different media.

Physical parameters	Values	Media	Loss of mass (%)
Real density (g/ml)	1.688 ± 0.012	HCl (33 %)	47.8
Apparent density (g/ml)	0.21 ± 0.15	NaOH (0.05 M)	34.0
Porosity (%)	87.67	NaCl (0.001 M)	42.0
Compressibility (%)	62.56	NaOCl (10 %)	39.4
Flow rate	0		
Effective diffusive ( $m^2/s^2$ ) (water molecule)	$1.02 \times 10^{-8}$		
Theoretical diffusivity ( $m^2/s^2$ )	$0.88 \times 10^{-7}$		
Tortuosity ( $\tau$ )	$1.79 \pm 0.11$		
Surface Area by MB method ( $m^2 g^{-1}$ )	124.88		
Mean pore volume ( $m^3/kg$ )	0.52		
Mean radius pore (m)	$8.32 \times 10^{-3}$		
Hollow fraction ( $F_h$ )	0.47		
Apparent ion exchange capacity (%)	86.20		

surface area, this material displayed adequate and like other silicate-based material properties [18], which characterize the good sorbent properties of  $MgOSiO_2 \cdot nH_2O$ .

### 3.3. Kinetic study of metals adsorption

Table 7 shows the adsorption capacity ( $q_e$ ), total lifetime ( $t$ ) and media lifetime ( $t_{1/2}$ ) for the four heavy metals under study. The adsorption was slightly faster for  $Mn^{2+}$  ions (29 min) but, with a lower adsorption capacity ( $15.12 \text{ mg g}^{-1}$ ) with respect to the other studied metal ions. The material displayed an equivalent adsorption capacity of  $25.10 \text{ mg g}^{-1}$  for  $Zn^{2+}$  and  $23.19 \text{ mg g}^{-1}$  for  $Co^{2+}$  ions. In the case of  $Cu^{2+}$ , the material displayed the highest adsorption capacity,  $58.89 \text{ mg g}^{-1}$ . The differences in adsorption capacity for the four heavy metals can be attributed to various factors, such as their ionic radii, hydration energy,

Table 7

Results of the material behavior in the presence of the studied metal ions.

Species	Ci (mg/L)	Ct (mg/L)	$q_e$ ( $\text{mg g}^{-1}$ )	t (min)	$t_{1/2}$ (min)
$Mn^{2+}$	0.598	0.548	15.12	29	14.5
$Co^{2+}$	0.960	0.883	23.19	32	7.6
$Cu^{2+}$	0.950	0.754	58.89	55	27.5
$Zn^{2+}$	0.592	0.508	25.10	58	29.0

and specific interactions with the adsorbent. This order is very similar to the radius of these metals in an octahedral environment with water ligands ( $r_H \text{Zn}^{2+} = 4.30 \text{ \AA}$ ,  $r_H \text{Cu}^{2+} = 4.19 \text{ \AA}$  and  $r_H \text{Mn}^{2+} = 4.38 \text{ \AA}$ ) [65], so that there would seem to be a marked influence of these properties on the sorption capacity of each adsorbate. In the case of the  $\text{Cu}^{2+}$ , the Jahn–Teller distortion [66] leads to a change in its structure enhancing its diffusion and interaction with the adsorbent resulting in a higher adsorption. The  $\text{Mn}^{2+}$  ions show a relatively larger radius, which can limit their diffusion rate and access to internal cavities in the adsorbent, leading to the lowest adsorption. The fast equilibrium of  $\text{Mn}^{2+}$  ions suggests that these ions cannot access the most internal cavities, reaching the adsorption equilibrium faster and resulting in low adsorption (does not saturate all the material). In the case of the  $\text{Zn}^{2+}$  and  $\text{Co}^{2+}$ , the adsorption capacity is equivalent because of these equivalent ionic radii. These results highlight the importance of the physicochemical properties of the metal ions in determining their adsorption behavior on silicate-based materials. They also suggest that the adsorbent may need to be optimized for each specific metal ion to achieve high adsorption efficiencies.

The kinetic results were evaluated through the determination coefficient ( $R^2$ ) of the different models studied for each ion. As shown in Table 8, the sorption process of the  $\text{Cu}^{2+}$ ,  $\text{Mn}^{2+}$ , and  $\text{Co}^{2+}$  adjusts, preferably to pseudo-second order and Elovich's models. These suggest that for these metal ions, the adsorption can be both chemical (chemisorption) and physical (physisorption) mechanisms. Based on the high value of the determination coefficient of the Elovich model ( $R^2 > 0.964$ ) it can be said that there are structural disorders in the silicate porous system, and its surface can be considered a heterogeneous system. The adsorption of  $\text{Mn}^{2+}$  on  $\text{MgOSiO}_2\text{nH}_2\text{O}$  is controlled by both chemical and physical adsorption involving the strong surface complexation of metal ions with the oxygen-containing groups on the surface of  $\text{MgO-SiO}_2\text{nH}_2\text{O}$ . In theoretical predictions, it was suggested that a possible reason is the characteristic ionic interaction patterns for the strong interaction of the four oxygen atoms with the  $\text{Mn}^{2+}$  in the  $\text{Mg}_2\text{O}_8\text{Si}_3\text{Mn}$  system. According to the intraparticle diffusion model, the  $\text{Mn}^{2+}$  displays the lowest dependence which agrees with this limit diffusion and access to internal cavities in the adsorbent. Regarding  $\text{Zn}^{2+}$ , a pseudo-first-order model adjusts, however, the intraparticle diffusion of the adsorbate must be considered. This indicates the speed at which  $\text{Zn}^{2+}$  ions can move into the adsorbent, which in turn influences the overall rate and efficiency of the adsorption process.

These results suggest that the  $\text{MgOSiO}_2\text{nH}_2\text{O}$  synthesized showed good physicochemical properties as a heavy metal ion sorbent in a water medium. However, it can be used restrictedly because its chemical characteristics are given moderate resistance to the different media (see Table 6). For this reason, their use is recommendable in a matrix with neutral pH. The kinetic study showed preferably chemical adsorption processes on a surface heterogeneity, without lateral interaction in  $\text{MgOSiO}_2\text{nH}_2\text{OMn}$ ,  $\text{MgOSiO}_2\text{nH}_2\text{OCo}$ , and  $\text{MgOSiO}_2\text{nH}_2\text{OCu}$  systems, and an exponential distribution of active sites. The intraparticle diffusion is an aspect to be considered for the  $\text{MgOSiO}_2\text{nH}_2\text{OZn}$  system. Indeed, adsorption is a complex process influenced by many factors. The nature of the adsorbent, such as its chemical composition, surface area, pore size distribution, and experimental conditions can significantly impact its adsorption capacity. Some experimental conditions of the system, including the adsorbent dose, temperature, pressure, pH, or multi-component systems (mixtures) can also affect the adsorption

process. For instance, higher temperatures can increase the rate of adsorption, while a change in pH can affect the charge of the adsorbent and the adsorbate, thus influencing their interaction. This study of heavy metal migration in multicomponent systems has not yet been addressed. Moreover, further experimental investigations are needed. This work is a preliminary basis where this material displayed good adsorption in the following sequence  $\text{Cu}^{2+} > \text{Zn}^{2+} \approx \text{Co}^{2+} > \text{Mn}^{2+}$  for which the ionic radii of the hydrated species should have a significant influence. Similar selectivity order results were reported by [22,66]. The synthesized silicate-based material shows a better or similar ability to remove heavy metals than other natural and synthetic materials reported (See Table 9). Therefore, this material can potentially be a highly effective alternative for removing heavy metals from wastewater.

### 3.4. Future remarks

In this research, the kinetic test was performed under controlled laboratory conditions which does not fully reproduce real-world conditions. Factors such as temperature, pH, multicomponent systems (presence of other pollutants), or an aqueous matrix complex (simulated or real industrial wastewater) can significantly affect the interaction between metals and  $\text{MgOSiO}_2\text{nH}_2\text{O}$ . So, an essential point will be that the next steps include multicomponent adsorption experiments [28]. In real-world applications, the adsorbent will often need to remove

**Table 9**  
Adsorption of heavy metal ions by different low-cost adsorbents.

Adsorbent material	Ions	Time (min)	$q_e$ (mg g <sup>-1</sup> )
Xanthate-modified magnetic chitosan [67]	$\text{Cu}^{2+}$	80	34.5
	$\text{Zn}^{2+}$	110	20.8
Aluminum silicate [18]	$\text{Co}^{2+}$	30	990
	$\text{Cu}^{2+}$	60	64
	$\text{Zn}^{2+}$	30	710
Asphaltenes/chitosan [68]	$\text{Mn}^{2+}$		60–80
	$\text{Zn}^{2+}$		
Albizia lebeck pods [5]	$\text{Zn}^{2+}$	30	4.84
	$\text{Cu}^{2+}$		3.12
Palygorskite [69]	$\text{Co}^{2+}$	180	8.8
	$\text{Mn}^{2+}$		0.85
Amorphous $\text{Al}(\text{OH})_3$	$\text{Cu}^{2+}$		104.09
	$\text{Fe}_3\text{O}_4/\text{graphene oxide}$ [71]		32.5
Fe $3\text{O}_4$ /chitosan/graphene oxide [72]			217.4
	Citrate modified Graphene Oxide (GO–C) [73]	$\text{Co}^{2+}$	145.35
Silicate porous material [74,75]	$\text{Cu}^{2+}$		32.26
	Zeolite	$\text{Cu}^{2+}$	3.5
Iron-coated zeolite [75]	$\text{Zn}^{2+}$		3.2
	$\text{Cu}^{2+}$		4.9
	$\text{Zn}^{2+}$		4.0
	$\text{Cu}^{2+}$	1440	0.48
	$\text{Zn}^{2+}$		0.45
Zeolite [65]	$\text{Mn}^{2+}$		0.44
	$\text{Cu}^{2+}$		10.8
Natural clay [76]	$\text{Mn}^{2+}$		1.56
	$\text{Co}^{2+}$		2.30
	$\text{Cu}^{2+}$		0.46
Magnesium ferrite gn- $\text{MgFe}_2\text{O}_4$ –300 [77]	$\text{Mn}^{2+}$	29	15.12
	$\text{Co}^{2+}$	32	23.19
	$\text{Cu}^{2+}$	55	58.89
	$\text{Zn}^{2+}$	58	25.10
$\text{MgOSiO}_2\text{nH}_2\text{O}$ (This study)	$\text{Mn}^{2+}$	29	15.12
	$\text{Co}^{2+}$	32	23.19
	$\text{Cu}^{2+}$	55	58.89
	$\text{Zn}^{2+}$	58	25.10

**Table 8**

Results of kinetic adsorption models of the heavy metals studied. The  $R^2$  is reported in parentheses and the numbers in bold correspond with the best adjustment.

Ions	Pseudo-first order	Pseudo-second order	Elovich	Intraparticle diffusion
$\text{Mn}^{2+}$	$y = -0.124x + 1.253$ (0.949)	$y = 0.162x + 0.364$ ( <b>0.997</b> )	$y = 0.998x + 2.518$ (0.964)	$y = 0.200x + 3.306$ (0.621)
$\text{Co}^{2+}$	$y = -2.0 \times 10^{-5}x - 0.986$ (0.806)	$y = 318.48x + 2430$ ( <b>0.996</b> )	$y = 0.001x + 0.0004$ ( <b>0.998</b> )	$y = 0.0001x + 0.001$ (0.846)
$\text{Cu}^{2+}$	$y = -0.0784x - 2.002$ (0.929)	$y = 5.616x + 28.481$ ( <b>0.999</b> )	$y = 0.027x + 0.061$ ( <b>0.994</b> )	$y = 0.003x + 0.108$ (0.747)
$\text{Zn}^{2+}$	$y = -0.026x + 6.265$ ( <b>0.987</b> )	$y = 1.0 \times 10^{-4}x + 0.105$ (0.822)	$y = 109.46x - 124.22$ (0.838)	$y = 17.533x + 12.819$ ( <b>0.986</b> )

multiple types of metal ions from the water. These different ions can compete for adsorption sites on the adsorbent, affecting its overall removal efficiency. By testing the adsorbent in multicomponent systems, you can evaluate this competition effect and adjust the doses and proportions of the silicate as needed to achieve the required removal efficiency. In addition, using a water matrix that is closer to actual industrial waters is another proposed step. This would involve introducing other substances typically found in industrial wastewater, which would provide a more accurate representation of the real-world conditions under which the adsorbent would be used [65,74]

Studies of desorption and reusability tests of the  $\text{MgOSiO}_2\text{nH}_2\text{O}$  are crucial too, because it affects the efficiency and cost-effectiveness. Previous study has demonstrated that the desorption process for  $\text{Cu}^{2+}$ ,  $\text{Zn}^{2+}$ , and  $\text{Mn}^{2+}$  ions onto zeolite behaves differently [65]. This could be beneficial in certain applications where selective adsorption and desorption are required. While the efficiency of multi-cycle spent adsorbents tends to decline over time, this is not an insurmountable challenge. With appropriate modifications and improvements, the efficacy of this adsorbent can be significantly enhanced. According to the features of the simulated industrial wastewater, one of the recommended processes is a primary treatment, which involves the precipitation of metals by adjusting the pH level. This is then followed by a secondary treatment of adsorption, where a  $\text{MgOSiO}_2\text{nH}_2\text{O}$  modified could be utilized as the material for adsorption. A way could be reported previously by Li et al.[78] that synthesized a silica-based material capable of adsorbing  $\text{Pb}^{2+}$ . The results demonstrated a maximum adsorption capacity of  $74.5 \text{ mg g}^{-1}$  for  $\text{Pb}^{2+}$ . After 5 cycles of adsorption-regeneration, the adsorption capacity of the reused adsorbent still reached 70.9 % (for  $\text{Pb}^{2+}$ ) of the initial value. The future steps could lie in the optimization of  $\text{MgOSiO}_2\text{nH}_2\text{O}$  regeneration processes, which could potentially revolutionize these heavy metals treatment methodologies by improving their economic and environmental efficiency. In addition, the chemical stability of regenerated adsorbents significant factor to consider [79]. The regeneration process may cause changes in the adsorbent's physical and chemical properties, such as surface area, pore size, and chemical composition. These changes can affect the adsorbent's adsorption capacity, selectivity, and lifetime. Therefore, it is necessary to investigate the chemical stability of regenerated  $\text{MgOSiO}_2\text{nH}_2\text{O}$ , including their resistance to chemical, and mechanical degradation. This can be done through various techniques, such as XPS, XRD, FTIR, and electron microscopy.

Results from adsorption studies conducted at a small scale may not always scale up predictably to larger systems. This can make it challenging to apply findings from laboratory studies to industrial-scale processes. The points mentioned are crucial for evaluating the practical applicability and effectiveness of  $\text{MgOSiO}_2\text{nH}_2\text{O}$  as an adsorbent for heavy metal removal. Therefore, while laboratory-scale adsorption studies provide valuable insights, careful consideration and additional research are often needed to successfully apply these findings to industrial-scale processes.

Despite these limitations, this research provides valuable insights into the interactions between several heavy metals and  $\text{MgOSiO}_2\text{nH}_2\text{O}$  material and guides the next steps for enhancing the efficacy of  $\text{MgOSiO}_2\text{nH}_2\text{O}$  material for heavy metal removal.

#### 4. Conclusions

This research underscores the potential of  $\text{MgOSiO}_2\text{nH}_2\text{O}$  material in heavy metal removal and highlights the need for continued research to optimize this material. The insights gained from this study will pave the way for the development of more efficient silicate-based adsorbents for heavy metal removal from wastewater. Here, the theoretical calculations were aimed at further investigating the nature of adsorption between four metal ions ( $\text{Cu}^{2+}$ ,  $\text{Zn}^{2+}$ ,  $\text{Co}^{2+}$  and  $\text{Mn}^{2+}$ ) and a silicate-based material. These computational calculations were carried out over a model of the building units of the system of interest, which consist of a

$\text{Mg}_2\text{O}_3\text{Si}_3$  cluster interacting with the target heavy metal ions. The results showed significant differences in the binding energy, which can be attributed to the different electronic structures and sizes of the cations, furthermore, revealed that the binding energy is not solely determined by the charge of the cation, but also by the specific interactions between the cation and the silicate-based material. The computational analysis of the adsorption energies indicates that the adsorption of four metal ions on the  $\text{Mg}_2\text{O}_3\text{Si}_3$  surface is energetically favorable in all cases. The synthetic  $\text{MgOSiO}_2\text{nH}_2\text{O}$  material displays beneficial chemical and physical properties as a metal ion sorbent in a water medium at neutral pH. The material exhibits good adsorption with the following sequence:  $\text{Cu}^{2+}$  ( $59 \text{ mg g}^{-1}$ ) >  $\text{Zn}^{2+}$  ( $25 \text{ mg g}^{-1}$ )  $\approx$   $\text{Co}^{2+}$  ( $23 \text{ mg g}^{-1}$ ) >  $\text{Mn}^{2+}$  ( $15 \text{ mg g}^{-1}$ ). Compared to other adsorbent materials, this eco-friendly material demonstrated a good ability to remove heavy metal ions, which suggests that our material may be a good alternative for wastewater treatment. The results provide information on the adsorption process and might be a useful tool to guide experimental efforts in the design of new silicate-based materials with better properties to remove interesting metal ions.

#### CRediT authorship contribution statement

**Lisdelys González-Rodríguez:** Writing – review & editing, Writing – original draft, Validation, Project administration, Methodology, Investigation, Formal analysis, Conceptualization. **Yoan Hidalgo-Rosa:** Writing – review & editing, Writing – original draft, Validation, Supervision, Methodology, Investigation, Formal analysis, Data curation. **Julio Omar Prieto García:** Supervision, Resources, Project administration, Funding acquisition, Formal analysis, Data curation. **Manuel A. Treto-Suárez:** Writing – review & editing, Writing – original draft, Validation, Supervision, Investigation, Formal analysis, Data curation. **Karel Mena-Ulecia:** Writing – original draft, Validation, Supervision, Project administration, Methodology, Formal analysis, Conceptualization. **Osvaldo Yañez:** Writing – review & editing, Visualization, Validation, Supervision, Software, Resources, Methodology, Investigation, Data curation.

#### Declaration of competing interest

The authors declare that they have no known competing financial interests or personal relationships that could have appeared to influence the work reported in this paper.

#### Data availability

Data will be made available on request.

#### Acknowledgments

The authors acknowledged the assistance from the Chemistry Department of Central University Martha Abreu de las Villas, Cuba. L. G-R says thanks to Duncan Hunter, Felipe H. Valenzuela, and Rocío Mora for sharing quality time and learning in the EULA adsorption laboratory. This work received the support of ANID Postdoctoral 3230141, and ANID/FONDAP/1522A0006. O.Y. acknowledges the UDLA-PIR202409. This research was partially supported by the supercomputing [infrastructure of the NLHPC (ECM-02)]. The authors thank the Editors and reviewers for their valuable comments and suggestions, which improved the quality of the paper.

#### Supplementary materials

Supplementary material associated with this article can be found, in the online version, at [doi:10.1016/j.chphi.2024.100714](https://doi.org/10.1016/j.chphi.2024.100714).

## References

- [1] M.G. Uddin, S. Nash, A.I. Olbert, A review of water quality index models and their use for assessing surface water quality, *Ecol. Indic.* 122 (2021), <https://doi.org/10.1016/j.ecolind.2020.107218>.
- [2] K. Mena-Ulecia, H.H. Hernández, Decentralized peri-urban wastewater treatment technologies assessment integrating sustainability indicators, *Water Sci. Technol.* 72 (2015) 214–222, <https://doi.org/10.2166/wst.2015.209>.
- [3] N. Akhtar, M.I. Syakir Ishak, S.A. Bhawani, K. Umar, Various natural and anthropogenic factors responsible for water quality degradation: a review, *Water (Switzerl.)* (2021) 13, <https://doi.org/10.3390/w13192660>.
- [4] A. Begum, M. Ramaiah, I.Khan Harikrishna, K. Veena, Heavy metal pollution and chemical profile of Cauvery river water, *E-J. Chem.* 6 (2009) 47–52, <https://doi.org/10.1155/2009/154610>.
- [5] S. Mustapha, D.T. Shuaib, M.M. Ndamitso, M.B. Etsuyankpa, A. Sumaila, U. M. Mohammed, M.B. Nasirudeen, Adsorption isotherm, kinetic and thermodynamic studies for the removal of Pb(II), Cd(II) and Cu(II) ions from aqueous solutions using Albizia lebeck pods, *Appl. Water. Sci.* 9 (2019), <https://doi.org/10.1007/s13201-019-1021-x>.
- [6] L. González-Rodríguez, J.O.P. García, L. Rodríguez-López, Y. Hidalgo-Rosa, M. A. Treto-Suárez, M.G. Enriquez, Á.M. Trujillo, Cassava Husk Powder as an Eco-Friendly Adsorbent for the Removal of Nickel (II) Ions, 2022, [https://doi.org/10.1007/978-3-030-88919-7\\_3](https://doi.org/10.1007/978-3-030-88919-7_3).
- [7] J. Pizarro, P.M. Vergara, J.A. Rodríguez, A.M. Valenzuela, Heavy metals in northern Chilean rivers: spatial variation and temporal trends, *J. Hazard. Mater.* 181 (2010) 747–754, <https://doi.org/10.1016/j.jhazmat.2010.05.076>.
- [8] A. Debnath, P.K. Singh, Y.C. Sharma, Metallic contamination of global river sediments and latest developments for their remediation, *J. Environ. Manag.* 298 (2021) 113378, <https://doi.org/10.1016/j.jenvman.2021.113378>.
- [9] Md.A. Alam, W.A. Shaikh, Md.O. Alam, T. Bhattacharya, S. Chakraborty, B. Show, I. Saha, Adsorption of As (III) and As (V) from aqueous solution by modified Cassia fistula (golden shower) biochar, *Appl. Water. Sci.* 8 (2018), <https://doi.org/10.1007/s13201-018-0839-y>.
- [10] N.R. Chereddy, S. Janakipriya, P.S. Korrapati, S. Thennarasu, A.B. Mandal, Solvent-assisted selective detection of sub-micromolar levels of Cu 2+ ions in aqueous samples and live-cells, *Analyst* 138 (2013) 1130–1136, <https://doi.org/10.1039/c2an36339a>.
- [11] K. Grzeszczak, S. Kwiatkowski, D. Kosik-Bogacka, The role of Fe, Zn, and Cu in pregnancy, *Biomolecules* 10 (2020) 1–33, <https://doi.org/10.3390/biom10081176>.
- [12] W.Hz.O, (WHO), *Manganese in Drinking-water*, 2011.
- [13] M.A. Renu, K. Singh, Heavy metal removal from wastewater using various adsorbents: a review, *J. Water Reuse Desalinat.* 7 (2017) 387–419, <https://doi.org/10.2166/wrd.2016.104>.
- [14] M.F. Attallah, I.M. Ahmed, M.M. Hamed, Treatment of industrial wastewater containing Congo Red and Naphthol Green B using low-cost adsorbent, *Environ. Sci. Pollut. Res.* 20 (2013) 1106–1116, <https://doi.org/10.1007/s11356-012-0947-4>.
- [15] J. Saleem, U. Bin Shahid, M. Hijab, H. Mackey, G. McKay, Production and applications of activated carbons as adsorbents from olive stones, *BioMass Convers. Biorefin.* 9 (2019) 775–802, <https://doi.org/10.1007/s13399-019-00473-7>.
- [16] M. Wolowicz, M. Komorowska-Kaufman, A. Pruss, G. Rzepa, T. Bajda, Removal of heavy metals and metalloids from water using drinking water treatment residuals as adsorbents: a review, *Minerals* 9 (2019), <https://doi.org/10.3390/min9080487>.
- [17] I.M. El-Naggar, M.M. Abou-Mesalam, Novel inorganic ion exchange materials based on silicates; synthesis, structure and analytical applications of magnesio-silicate and magnesium aluminosilicate sorbents, *J. Hazard. Mater.* 149 (2007) 686–692, <https://doi.org/10.1016/j.jhazmat.2007.04.029>.
- [18] M.A. Treto-Suárez, J.O. Prieto-García, Á. Mollineda-Trujillo, E. Lamazares, Y. Hidalgo-Rosa, K. Mena-Ulecia, Kinetic study of removal heavy metal from aqueous solution using the synthetic aluminum silicate, *Sci. Rep.* 10 (2020) 1–12, <https://doi.org/10.1038/s41598-020-67720-0>.
- [19] B. Kussainova, G. Tazhkenova, I. Kazarinov, A. Nurlybayeva, A. Lamichova, L. Kusepova, T. Mashan, B. Tantybayeva, B. Saurbayeva, G. Seitbekova, D. Kulbayeva, R. Kudaibergenova, Comparative study of the physico-chemical properties of sorbents based on natural bentonites modified with iron (III) and aluminium (III) polyhydroxocations, *Coatings* 13 (2023), <https://doi.org/10.3390/coatings13111974>.
- [20] M. Xu, J. Wang, J. Wu, Recent advances of silicate materials for wastewater treatment: a review, *Mater. Res. Express.* 11 (2024), <https://doi.org/10.1088/2053-1591/ad2c63>.
- [21] X. Fan, H. Liu, E. Anang, D. Ren, Effects of electronegativity and hydration energy on the selective adsorption of heavy metal ions by synthetic nax zeolite, *Mater. (Basel)* 14 (2021), <https://doi.org/10.3390/ma14154066>.
- [22] M.K. Doula, Simultaneous removal of Cu, Mn and Zn from drinking water with the use of clinoptilolite and its Fe-modified form, *Water Res.* 43 (2009) 3659–3672, <https://doi.org/10.1016/j.watres.2009.05.037>.
- [23] G. Gao, T. Sun, Y. Sun, Y. Xu, X. Liang, Adsorption of Cd(II) on mercaptopylorskite functional materials with different proportions: performance, mechanism and DFT study, *J. Clean. Prod.* 452 (2024), <https://doi.org/10.1016/j.jclepro.2024.142052>.
- [24] S. Singh, S. Koley, B. Modak, M. Amarnath, H. Basu, C.N. Patra, Synthesis of amine functionalized SiO<sub>2</sub> microspheres loaded polymeric hydrogel and its application for simultaneous evicting of divalent metal ions (Pb<sup>2+</sup>, Cd<sup>2+</sup>, Cu<sup>2+</sup> and Ni<sup>2+</sup>), *Mater. Today Chem.* 33 (2023) 101720, <https://doi.org/10.1016/j.mtchem.2023.101720>.
- [25] R. Huang, L. He, T. Zhang, D. Li, P. Tang, Y. Zhao, Y. Feng, Fabrication and adsorption behavior of magnesium silicate hydrate nanoparticles towards methylene blue, *Nanomaterials* 8 (2018), <https://doi.org/10.3390/nano8050271>.
- [26] Y. An, W. Zhang, H. Liu, Y. Zhong, Z. Hu, Y. Shao, Z. Chen, Y. Ren, B. Wang, S. Wang, X. Zhang, X. Wang, Lignocellulose-based superabsorbent polymer gel crosslinked with magnesium aluminum silicate for highly removal of Zn (II) from aqueous solution, *Polym. (Basel)* (2021) 13, <https://doi.org/10.3390/polym13234161>.
- [27] X. Yan, Q. Zhang, Q. Rao, S. Chen, X. Wang, W. Song, L. Cheng, S. Guan, W. Song, Efficient removal of nonylphenol contamination from water using optimized magnesium silicate, *Mater. (Basel)* 15 (2022), <https://doi.org/10.3390/ma15134445>.
- [28] A.I. Ivanets, N.V. Kitikova, I.L. Shashkova, M.Yu. Roshchina, V. Srivastava, M. Sillanpää, Adsorption performance of hydroxyapatite with different crystalline and porous structure towards metal ions in multicomponent solution, *J. Water. Process. Eng.* 32 (2019) 100963, <https://doi.org/10.1016/j.jwpe.2019.100963>.
- [29] K. Gong, K. Yang, C.E. White, Density functional modeling of the binding energies between aluminosilicate oligomers and different metal cations, *Front. Mater.* 10 (2023) 1–17, <https://doi.org/10.3389/fmats.2023.1089216>.
- [30] R.F.W. Bader, A quantum theory of molecular structure and its applications, *Chem. Rev.* 91 (1991) 893–928, <https://doi.org/10.1021/cr00005a013>.
- [31] C.M. Breneman, K.B. Wiberg, Determining atom-centered monopoles from molecular electrostatic potentials. The need for high sampling density in formamide conformational analysis, *J. Comput. Chem.* 11 (1990) 361–373, <https://doi.org/10.1002/jcc.540110311>.
- [32] T. Lu, Q. Chen, Independent gradient model based on Hirshfeld partition: a new method for visual study of interactions in chemical systems, *J. Comput. Chem.* 43 (2022) 539–555, <https://doi.org/10.1002/jcc.26812>.
- [33] A.E. Reed, R.B. Weinstock, F. Weinhold, Natural population analysis, *J. Chem. Phys.* 83 (1985) 735–746, <https://doi.org/10.1063/1.449486>.
- [34] O. Yañez, R. Báez-Grez, D. Inostroza, R. Pino-Ríos, W.A. Rabanal-León, J. Contreras-García, C. Cardenas, W. Tiznado, Kick–Fukui: a Fukui function-guided method for molecular structure prediction, *J. Chem. Inf. Model.* 61 (2021) 3955–3963, <https://doi.org/10.1021/acs.jcim.1c00605>.
- [35] L. González-Rodríguez, O. Yañez, K. Mena-Ulecia, Y. Hidalgo-Rosa, X. García-Carmona, C. Ulloa-Tesser, Exploring the adsorption of five emerging pollutants on activated carbon: a theoretical approach, *J. Environ. Chem. Eng.* 12 (2024), <https://doi.org/10.1016/j.jece.2024.112911>.
- [36] M.A. Adicoat, G.F. Metha, Kick: constraining a stochastic search procedure with molecular fragments, *J. Comput. Chem.* 30 (2009) 57–64, <https://doi.org/10.1002/jcc.21026>.
- [37] O. Yañez, V. García, J. Garza, W. Orellana, A. Vásquez-Espinal, W. Tiznado, (Li 6 Si 2)–5: The Smallest Cluster-Assembled Materials Based on Aromatic Si 56– Rings, *Chemistry - A European Journal* 25 (2019) 2467–2471, <https://doi.org/10.1002/chem.201805677>.
- [38] C. Adamo, V. Barone, Toward reliable density functional methods without adjustable parameters: the PBE0 model, *J. Chem. Phys.* 110 (1999) 6158–6170, <https://doi.org/10.1063/1.478522>.
- [39] P. Fuentealba, L. Von Szentpily, H. Preuss, H. Stoll, Pseudopotential Calculations for Alkaline-Earth Atoms, 1985. <http://iopscience.iop.org/0022-3700/18/7/010>.
- [40] H. Schröder, A. Creon, T. Schwabe, Reformulation of the D3(Becke-Johnson) dispersion correction without resorting to higher than C6 dispersion coefficients, *J. Chem. Theory. Comput.* 11 (2015) 3163–3170, <https://doi.org/10.1021/acs.jctc.5b00400>.
- [41] F. Weigend, R. Ahlrichs, Balanced basis sets of split valence, triple zeta valence and quadruple zeta valence quality for H to Rn: design and assessment of accuracy, *Phys. Chem. Chem. Phys.* 7 (2005) 3297–3305, <https://doi.org/10.1039/b508541a>.
- [42] M.J. Frisch, G.W. Trucks, H.B. Schlegel, G.E. Scuseria, M.A. Robb, J.R. Cheeseman, G. Scalmani, V. Barone, B. Mennucci, G.A. Petersson, H. Nakatsuji, M. Caricato, X. Li, H.P. Hratchian, A.F. Izmaylov, J. Bloino, G. Zheng, J.L. Sonnenberg, M. Hada, M. Ehara, K. Toyota, R. Fukuda, J. Hasegawa, M. Ishida, T. Nakajima, Y. Honda, O. Kitao, H. Nakai, T. Vreven, J.A. Montgomery, J.E. Peralta, F. Ogliaro, M. Bearpark, J.J. Heyd, E. Brothers, K.N. Kudin, V.N. Staroverov, R. Kobayashi, J. Normand, K. Raghavachari, A. Rendell, J.C. Burant, S.S. Iyengar, J. Tomasi, M. Cossi, N. Rega, J.M. Millam, M. Klene, J.E. Knox, J.B. Cross, V. Bakken, C. Adamo, J. Jaramillo, R. Gomperts, R.E. Stratmann, O. Yazyev, A.J. Austin, R. Cammi, C. Pomelli, J.W. Ochterski, R.L. Martin, K. Morokuma, V.G. Zakrzewski, G.A. Voth, P. Salvador, J.J. Dannenberg, S. Dapprich, A.D. Daniels, Farkas, J. B. Foresman, J.V. Ortiz, J. Cioslowski, D.J. Fox, Gaussian 09, Revision C.01, Gaussian 09, Revision C.01, Gaussian, Inc., Wallingford CT, 2010.
- [43] K.B. Wiberg, Application of the pople-santry-segal CNDO method to the cyclopropylcarbanyl and cyclobutyl cation and to bicyclobutane, *Tetrahedron* 24 (1968) 1083–1096, [https://doi.org/10.1016/0040-4020\(68\)88057-3](https://doi.org/10.1016/0040-4020(68)88057-3).
- [44] R.P. Gangadharana, S.S. Krishnanb, Natural Bond Orbital (NBO) population analysis of 1-azanaphthalene-8-ol, *Acta Phys. Pol.* a 125 (2014) 18–22, <https://doi.org/10.12693/APhysPolA.125.18>.
- [45] T. Lu, F. Chen, Multiwfn: a multifunctional wavefunction analyzer, *J. Comput. Chem.* 33 (2012) 580–592, <https://doi.org/10.1002/jcc.22885>.
- [46] H. Bader, The characterization of atomic interactions, *J. Chem. Phys.* 80 (1984) 1943–1960.
- [47] R.F.W. Bader, *Atoms in molecules: a Quantum Theory*, Clarendon Press, 1990. <https://globaloup.com/academic/product/atoms-in-molecules-9780198558651#.WyrPmDy72k4.mendeley> (accessed June 19, 2018).

- [48] K. Granados-Tavera, M. Zambrano-Angulo, Y. Hidalgo-Rosa, X. Zarate, G. Cárdenas-Jirón, Tuning the visible-NIR absorption of azulocyanine-based photosensitizers, *J. Mol. Model.* 28 (2022) 1–13, <https://doi.org/10.1007/S00894-022-05329-Y/TABLES/5>.
- [49] M. Zhao, S. Li, M. Wang, X. Guan, R. Zhao, Adsorption of water and formic acid molecules on the (104) surface of calcite: a theoretical study by DFT-D3, *New J. Chem.* 47 (2023) 8737–8743, <https://doi.org/10.1039/d3nj00925d>.
- [50] M. Munir, F. Ahsan, M. Yar, K. Ayub, Theoretical investigation of double-cubed polycationic cluster (Sb<sub>7</sub>Se<sub>8</sub>Cl<sub>2</sub>)<sub>3</sub><sup>+</sup> for the storage of helium and neon, *Mater. Sci. Semicond. Process.* 148 (2022) 106756, <https://doi.org/10.1016/j.mssp.2022.106756>.
- [51] R.F. Michael Clugston, *Advanced Chemistry - Michael Clugston, Rosalind Flemming* - Google Books, OUP Oxford, 2000, pp. 262–263.
- [52] S. Lowell, J.E. Shields, M.A. Thomas, M. Thommes, *Characterization of Porous Solids and powders: Surface area, Pore Size and Density*, Kluwer Academic Publishers, New York, 2004, <https://doi.org/10.1007/978-1-4020-2303-3>.
- [53] N.N. Mohsenin, *Physical Properties of Plant and Animal Materials*, Edición., New York., 1970.
- [54] J.C. Santamarina, K.A. Klein, Y.H. Wang, E. Prencke, Specific surface: determination and relevance, *Canad. Geotechn. J.* 39 (2002) 233–241, <https://doi.org/10.1139/t01-077>.
- [55] A. Mauri, V. Consonni, M. Pavan, R. Todeschini, M. Chemometrics, DRAGON software: an easy approach to molecular descriptor calculations, *MATCH Commun. Mathematical. Comput. Chem.* (2006).
- [56] B. Qiu, X. Tao, H. Wang, W. Li, X. Ding, H. Chu, Biochar as a low-cost adsorbent for aqueous heavy metal removal: a review, *J. Anal. Appl. Pyrolysis.* 155 (2021) 105081, <https://doi.org/10.1016/j.jaap.2021.105081>.
- [57] J.P. Simonin, On the comparison of pseudo-first order and pseudo-second order rate laws in the modeling of adsorption kinetics, *Chem. Eng. J.* 300 (2016) 254–263, <https://doi.org/10.1016/j.cej.2016.04.079>.
- [58] F.C. Wu, R.L. Tseng, R.S. Juang, Initial behavior of intraparticle diffusion model used in the description of adsorption kinetics, *Chem. Eng. J.* 153 (2009) 1–8, <https://doi.org/10.1016/j.cej.2009.04.042>.
- [59] RS Team, RStudio: integrated development environment for R, (n.d.). <http://www.rstudio.com/> (accessed August 12, 2024).
- [60] M.D. Gould, C. Taylor, S.K. Wolff, G.S. Chandler, D. Jayatilaka, A definition for the covalent and ionic bond index in a molecule : AAAAn approach based on Roby's atomic projection operators, *Theor. Chem. Acc.* 119 (2008) 275–290, <https://doi.org/10.1007/s00214-007-0282-x>.
- [61] C. Tantardini, A.R. Oganov, Thermochemical electronegativities of the elements, *Nat. Commun.* 12 (2021) 1–9, <https://doi.org/10.1038/s41467-021-22429-0>.
- [62] P. Yu, R.J. Kirkpatrick, B. Poe, P.F. McMillan, X. Cong, Structure of calcium silicate hydrate (C-S-H): near-, mid-, and far-infrared spectroscopy, *J. Am. Ceram. Soc.* 82 (1999) 742–748.
- [63] C. Kannan, K. Muthuraja, M.R. Devi, Hazardous dyes removal from aqueous solution over mesoporous aluminophosphate with textural porosity by adsorption, *J. Hazard. Mater.* 244–245 (2013) 10–20, <https://doi.org/10.1016/j.jhazmat.2012.11.016>.
- [64] C.R.C.T. Zhang, L.J. Vandepierre, Development of magnesium silicate hydrate cement system for nuclear waste encapsulation, in: *NUWCEM*, Avignon, 2011: pp. 582–591.
- [65] A. Zendelska, M. Golomeova, G.B. Zendelska, Effect of competing cations (Cu, Zn, Mn, Pb) adsorbed by zeolite bearing tuff from Macedonia, *Nat. Environ. Pollut. Technol.* 17 (2018) 21–24.
- [66] J. Conradie, Jahn-Teller effect in high spin d4 and d9 octahedral metal-complexes, *Inorganica Chim. Acta* 486 (2019) 193–199, <https://doi.org/10.1016/j.ica.2018.10.040>.
- [67] R. Erdoo Kukwa, D. Tyoker Kukwa, A. David Oklo, T. Thaddeus Ligom, B. Ishwah, J. Ajegi Omenka, Adsorption studies of silica adsorbent using rice husk as a base material for metal ions removal from aqueous solution, *Am. J. Chem. Eng.* 8 (2020) 48, <https://doi.org/10.11648/j.ajche.20200802.12>.
- [68] A. Moktar, M. Daaou, A. Bendraoua, A. Morsli, Study of Cu<sup>2+</sup>, Zn<sup>2+</sup> and Mn<sup>2+</sup> ions adsorption using asphaltenes-chitosan composite beads, *Mater. Today Commun.* 33 (2022) 104928, <https://doi.org/10.1016/j.mtcomm.2022.104928>.
- [69] R. Baby, B. Saifullah, M.Z. Hussein, Palm Kernel Shell as an effective adsorbent for the treatment of heavy metal contaminated water, *Sci. Rep.* 9 (2019), <https://doi.org/10.1038/s41598-019-55099-6>.
- [70] Y. Ren, N. Yan, J. Feng, J. Ma, Q. Wen, N. Li, Q. Dong, Adsorption mechanism of copper and lead ions onto graphene nanosheet/δ-MnO<sub>2</sub>, *Mater. Chem. Phys.* 136 (2012) 538–544, <https://doi.org/10.1016/j.mtchemphys.2012.07.023>.
- [71] Z.-F. Yang, L.-Y. Li, C.-T. Hsieh, R.-S. Juang, Y.A. Gandomi, Fabrication of magnetic iron Oxide@Graphene composites for adsorption of copper ions from aqueous solutions, *Mater. Chem. Phys.* 219 (2018) 30–39, <https://doi.org/10.1016/j.matchemphys.2018.07.053>.
- [72] H. Hosseinzadeh, S. Ramin, Effective removal of copper from aqueous solutions by modified magnetic chitosan/graphene oxide nanocomposites, *Int. J. Biol. Macromol.* 113 (2018) 859–868, <https://doi.org/10.1016/j.ijbiomac.2018.03.028>.
- [73] A.I. Abd-Elhamid, E.M.A. Elgoud, Sh.Sh. Emam, H.F. Aly, Superior adsorption performance of citrate modified graphene oxide as nano material for removal organic and inorganic pollutants from aqueous solution, *Sci. Rep.* 12 (2022) 9204, <https://doi.org/10.1038/s41598-022-13111-6>.
- [74] D. Ouyang, Y. Zhuo, L. Hu, Q. Zeng, Y. Hu, Z. He, Research on the adsorption behavior of heavy metal ions by porous material prepared with silicate tailings, *Minerals* 9 (2019), <https://doi.org/10.3390/min9050291>.
- [75] T.C. Nguyen, P. Loganathan, T.V. Nguyen, S. Vigneswaran, J. Kandasamy, R. Naidu, Simultaneous adsorption of Cd, Cr, Cu, Pb, and Zn by an iron-coated Australian zeolite in batch and fixed-bed column studies, *Chem. Eng. J.* 270 (2015) 393–404, <https://doi.org/10.1016/j.cej.2015.02.047>.
- [76] L.M. Zaccaroni, Z.M. Magriotis, M. das G. Cardoso, W.D. Santiago, J.G. Mendonça, S.S. Vieira, D.L. Nelson, Natural clay and commercial activated charcoal: properties and application for the removal of copper from cachaça, *Food Control* 47 (2015) 536–544, <https://doi.org/10.1016/j.foodcont.2014.07.035>.
- [77] A. Ivanets, V. Prozorovich, M. Roshchina, T. Kouznetsova, N. Budeiko, L. Kulbitskaya, A. Hosseini-Bandegharai, V. Masindi, V. Pankov, A comparative study on the synthesis of magnesium ferrite for the adsorption of metal ions: insights into the essential role of crystallite size and surface hydroxyl groups, *Chem. Eng. J.* 411 (2021) 128523, <https://doi.org/10.1016/j.cej.2021.128523>.
- [78] Z. Li, X. Tang, K. Liu, J. Huang, Q. Peng, M. Ao, Z. Huang, Fabrication of novel sandwich nanocomposite as an efficient and regenerable adsorbent for methylene blue and Pb (II) ion removal, *J. Environ. Manage* 218 (2018) 363–373, <https://doi.org/10.1016/j.jenvman.2018.04.082>.
- [79] R. Shahrokhi-Shahraki, C. Benally, M.G. El-Din, J. Park, High efficiency removal of heavy metals using tire-derived activated carbon vs commercial activated carbon: insights into the adsorption mechanisms, *Chemosphere* 264 (2021) 128455, <https://doi.org/10.1016/j.chemosphere.2020.128455>.